Title
Structure-based discovery of opioid analgesics with reduced side effects

Permalink
https://escholarship.org/uc/item/41j4g4rn

Journal
Nature, 537(7619)

ISSN
0028-0836

Authors
Manglik, Aashish
Lin, Henry
Aryal, Dipendra K
et al.

Publication Date
2016-09-01

DOI
10.1038/nature19112

Peer reviewed

Structure–based discovery of opioid analgesics with reduced side effects

Aashish Manglik[1,*], **Henry Lin**[2,*], **Dipendra K. Aryal**[3,*], **John D. McCorvy**[3], **Daniela Dengler**[4], **Gregory Corder**[5], **Anat Levit**[2], **Ralf C. Kling**[4,6], **Viachaslau Bernat**[4], **Harald Hübner**[4], **Xi-Ping Huang**[3], **Maria F. Sassano**[3], **Patrick M. Giguère**[3], **Stefan Löber**[4], **Da Duan**[2], **Grégory Scherrer**[1,5], **Brian K. Kobilka**[1], **Peter Gmeiner**[4], **Bryan L. Roth**[3], and **Brian K. Shoichet**[2]

[1]Department of Molecular and Cellular Physiology, Stanford University School of Medicine, Stanford, California 94305, USA

[2]Department of Pharmaceutical Chemistry, University of California, San Francisco, California 94158, USA

[3]Department of Pharmacology, UNC Chapel Hill Medical School, Chapel Hill, North Carolina 27514, USA

[4]Department of Chemistry and Pharmacy, Friedrich-Alexander-Universität Erlangen-Nürnberg, Schuhstraße 19, 91052 Erlangen, Germany

[5]Department of Anesthesiology, Perioperative and Pain Medicine, Neurosurgery, Stanford Neurosciences Institute, Stanford University School of Medicine, Stanford, California 94305, USA

[6]Institut für Physiologie und Pathophysiologie, Paracelsus Medical University, 90419 Nuremberg, Germany

Abstract

Morphine is an alkaloid from the opium poppy used to treat pain. The potentially lethal side effects of morphine and related opioids—which include fatal respiratory depression—are thought to be mediated by μ-opioid-receptor (μOR) signalling through the β-arrestin pathway or by actions at other receptors. Conversely, G-protein μOR signalling is thought to confer analgesia. Here we computationally dock over 3 million molecules against the μOR structure and identify new scaffolds unrelated to known opioids. Structure-based optimization yields PZM21—a potent G_i activator with exceptional selectivity for μOR and minimal β-arrestin-2 recruitment. Unlike morphine, PZM21 is more efficacious for the affective component of analgesia versus the reflexive component and is devoid of both respiratory depression and morphine-like reinforcing activity in mice at equi-analgesic doses. PZM21 thus serves as both a probe to disentangle μOR signalling and a therapeutic lead that is devoid of many of the side effects of current opioids.

Opiate addiction, compounded by the potentially lethal side effects of opiates such as respiratory depression, has driven optimization campaigns for safer and more effective analgesics since the 19th century. Although the natural products morphine and codeine, and the semi-synthetic drug heroin, are more reliably effective analgesics than raw opium, they retain its liabilities. The classification of opioid receptors into μ, δ, and κ and nociception subtypes[1,2] raised hopes that subtype-specific molecules would lack the liabilities of morphinan-based opiates. Despite the introduction of potent synthetic opioid agonists like methadone and fentanyl, and the discovery of endogenous opioid peptides[3], developing analgesics without the drawbacks of classic opioids has remained an elusive goal. Recent studies have suggested that opioid-induced analgesia results from μOR signalling through the G protein G_i, while many side effects, including respiratory depression and constipation, may be conferred via β-arrestin pathway signalling downstream of μOR activation (Fig. 1a)[4–6]. Agonists specific to the μOR and biased towards the G_i signalling pathway are therefore sought both as therapeutic leads and as molecular probes to understand μOR signalling. Recent progress has supported the feasibility and potential clinical utility of such biased μOR agonists[7,8].

The determination of the crystal structures of the μ, δ, κ and nociceptin opioid receptors[9–12] (Fig. 1b, c) provided an opportunity to seek new μOR agonists via structure-based approaches. Recent discovery campaigns have used crystal structures of other Family A G-protein-coupled receptors (GPCRs) to computationally dock large libraries of molecules, identifying ligands with new scaffolds and with nanomolar-range potencies[13–17]. We thus targeted the μOR for structure-based docking, seeking ligands with new chemotypes. We reasoned that such new chemotypes might confer signalling properties with new biological effects, as has been true for other structure-based campaigns[18,19].

Structure-based docking to the μOR

We docked over 3 million commercially available lead-like compounds[20] against the orthosteric pocket of inactive μOR[9], prioritizing ligands that interact with known affinity-determining residues and with putative specificity residues that differ among the four opioid receptor subtypes (Fig. 1b, d). For each compound, an average of 1.3 million configurations

was evaluated for complementarity to the receptor using the physics-based energy function[21] in DOCK3.6. As is common in docking[22,23] and screening, the top ranking molecules were inspected for features not explicitly captured in the scoring function. We manually examined the top 2,500 (0.08%) docked molecules for their novelty, their interactions with key polar residues such as Asp147[3.32] (superscripts indicate Ballesteros-Weinstein numbering[24]), and deprioritized those that showed conformational strain (a term occasionally poorly modelled by the scoring function). Ultimately, 23 high-scoring molecules with ranks ranging from 237 to 2,095 out of the over 3 million docked were selected for testing (Fig. 1e). Compared to the 5,215 μOR ligands annotated in ChEMBL16[25], these docking hits had Extended Connectivity Fingerprint 4 (ECFP4)-based Tanimoto coefficients (T_c) ranging from 0.28 to 0.31, which is consistent with the exploration of novel scaffolds[26]. Of the 23 tested, seven had μOR binding affinities (K_i) ranging from 2.3 μM to 14 μM (Extended Data Table 1, Extended Data Fig. 1).

The new ligands are predicted to engage the μOR in new ways (Fig. 1f and Extended Data Fig. 1). Most opioid ligands use a cationic amine to ion-pair with Asp147[3.32], a canonical interaction[27] observed in structures of the μOR, δOR, κOR and nociceptin receptor bound to ligands of different scaffolds[9–12,28]. As anticipated, the docked ligands recapitulated this interaction. Much less precedence exists for the formation of an additional hydrogen bond with this anchor aspartate, often mediated in the docking poses by a urea amide. In several of the new ligands the urea carbonyl is modelled to hydrogen bond with Tyr148[3.33], while the rest of the ligands often occupy sites unexplored by morphinans (Extended Data Fig. 1). To our knowledge, the double hydrogen bond coordination of Asp147[3.32] modelled in the docking poses has not been anticipated or observed previously for opioid ligands, and only 50 of the 5,215 annotated opioid ligands in ChEMBL16 contain a urea group.

Despite the structural novelty of the initial docking hits, their affinities were low. To enhance binding and selectivity, we docked 500 analogues of compounds **4**, **5** and **7** that retained the key recognition groups but added packing substituents or extended further towards the extracellular side of the receptor, where the opioid receptors are more variable. Of the 15 top-scoring analogues that were tested, seven had K_i values between 42 nM and 4.7 μM (Extended Data Table 2). Encouragingly, several were specific for the μOR over κOR (compounds **12**–**15**, Extended Data Table 2). We then investigated the more potent analogues for signalling potency and efficacy. Although the structure we docked against was the inactive state of the μOR, compounds **8** and **12**–**14** activated $G_{i/o}$ (Extended Data Table 2). A similar enrichment for agonists was previously seen in a docking study against the inactive state of the κOR[23], perhaps reflecting the small changes in the orthosteric pocket associated with opioid receptor activation[29]. Encouragingly, the most potent compound, **12** (Fig. 2a, b), strongly activated $G_{i/o}$ with low levels of β-arrestin-2 recruitment (Fig. 2c, d).

Structure-guided synthetic optimization

To optimize compound **12**, we synthesized stereochemically pure isomers and introduced a phenolic hydroxyl (Fig. 3a). The synthesis of the (*S*,*S*) stereoisomer of **12** improved affinity (K_i) to 4.8 nM and had a signalling EC_{50} of 65 nM; it was the most potent and efficacious $G_{i/o}$ signalling agonist among the four isomers (Fig. 3e). The phenolic hydroxyl, introduced

to make compound (S,S)-**21**, was designed to exploit a water-mediated hydrogen bond with His297[6.52], an interaction observed in the structure of μOR in complex with β-funaltrexamine (β-FNA) (Fig. 3b) and in other structures of the δOR[28] and κOR[11]. This hydroxyl was readily accommodated in the docked μOR-**12** complex, improving the predicted docking energy (Fig. 3c). Compound (S,S)-**21** had an EC_{50} of 4.6 nM in a $G_{i/o}$ activation assay, with 76% efficacy (Fig. 3f), and a K_i of 1.1 nM in radioligand binding assays (Extended Data Table 3), an improvement of 40-fold versus **12**. The other three stereoisomers of (S,S)-**21** were much less potent or efficacious (Extended Data Fig. 2a, b), suggesting a specific stereochemical requirement for both potency and efficacy in agreement with the docked poses[29] of (S,S)-**21** to the inactive and active structures of μOR (Fig. 3c, Extended Data Fig. 2c, d). We refer to (S,S)-**21** as compound PZM21 henceforth.

Because PZM21 was discovered against the inactive structure of μOR, its docked complex to active μOR retains ambiguities. To investigate its receptor-bound structure further, more detailed docking and molecular dynamics simulations were conducted. The resulting model was tested by synthesizing molecules that either perturbed or exploited specific modelled interactions (Fig. 3c, d, Extended Data Figs 2 and 3). Neutralization of charge by amidation (compound PZM28) decreases potency by 1,000-fold, supporting a key ionic interaction between the PZM21 tertiary amine and Asp147[3.32] (Fig. 3d and Extended Data Fig. 3). Compound PZM27, which adds steric bulk to the tertiary amine, was synthesized to disrupt putative hydrophobic interactions between the N-methyl group and Met151[3.36] and Trp293[6.48], consistent with its 30-fold loss of potency and decreased efficacy (Fig. 3d and Extended Data Fig. 3). Compounds PZM23, PZM24 and PZM25, which were synthesized to disrupt hydrogen bonding interactions in the model between the urea and Asp147[3.32], Tyr326[7.43] and Gln124[2.60], lose between 30- and 230-fold potency despite their decreased solvation penalties (Fig. 3d and Extended Data Fig. 3). These key ionic and hydrogen-bonding interactions are maintained for 3 μs of molecular dynamics simulations of PZM21 in complex with active μOR, as are interactions between the phenolic hydroxyl and the bridging waters to His297[6.52], further supporting their relevance to the modelled pose (Extended Data Fig. 2g). The thiophene of PZM21, modelled to fit in the more open specificity region of the μOR, can be replaced with a larger benzothiophene without loss of potency (Extended Data Fig. 3). Interactions of this thiophene with residues that differ among the opioid receptor sub-types may contribute to PZM21 specificity (Extended Data Fig. 2e). More compellingly, the simulations and docking predict that the PZM21 thiophene comes within 6 Å of Asn127[2.63] in the active μOR (Extended Data Fig. 2g). Accordingly, we synthesized an irreversible version of PZM21 (compound PZM29) designed to form a covalent bond with μOR engineered with an N127C mutation. Compound PZM29 binds irreversibly to this mutant but not the wild-type receptor and retains its efficacy as an agonist (Extended Data Fig. 3), supporting the overall orientation of PZM21 as modelled and simulated in the orthosteric μOR site.

PZM21 is a selective G_i-biased μOR agonist

PZM21 had no detectable κOR or nociceptin receptor agonist activity—it is actually an 18 nM κOR antagonist—while it is a 500-fold weaker δOR agonist (Extended Data Fig. 4 and Extended Data Table 3), making it a selective μOR agonist. To investigate specificity more

broadly, PZM21 was counter-screened for agonism against 316 other GPCRs[30]. Activity at 10µM was observed at several peptide and protein receptors; however, no potent activity was confirmed with a full dose–response experiment at these receptors. PZM21 therefore has high agonist specificity among GPCRs (Extended Data Fig. 5a–c). PZM21 was also tested for inhibition of the hERG ion channel and the dopamine, norepinephrine and serotonin neurotransmitter transporters. At hERG, PZM21 had an IC_{50} of between 2 and 4 µM, 500- to 1,000-fold weaker than its potency as a µOR agonist (Extended Data Fig. 5d). Its inhibition of the neurotransmitter transporters, which are also analgesia targets, was even weaker with IC_{50} values ranging from 7.8 to 34 µM (Extended Data Fig. 5e). Thus, PZM21 is a potent, selective, and efficacious µ opioid agonist.

A major goal of this study was to find new chemotypes that might display biased signalling and perhaps, unlike canonical opioid drugs, have more favourable *in vivo* profiles. Signalling by PZM21 and other µOR agonists appears to be mediated primarily by the heterotrimeric G protein $G_{i/o}$, as its effect on cAMP levels was eliminated by pertussis toxin and no activity was observed in a calcium release assay (Extended Data Fig. 6a–d). A maximal concentration of PZM21 led to no detectable β-arrestin-2 recruitment in the PathHunter assay (DiscoverRx) (Fig. 3g and Extended Data Fig. 6c) and a minimal level of µOR internalization compared to DAMGO and morphine (Extended Data Fig. 6e). Indeed, β-arrestin-2 recruitment was too low to even permit a formal calculation of bias[31], which quantifies the preference for one signalling pathway over another. Since β-arrestin recruitment can depend on the expression level of G protein-coupled receptor kinase 2 (GRK2)[32], we also investigated $G_{i/o}$ signalling and arrestin recruitment in cells co-transfected with this kinase. Even in the presence of overexpressed GRK2, PZM21 still has weak arrestin recruitment efficacy compared to DAMGO and even to morphine (Extended Data Fig. 6g–i). In fact, the signalling bias of PZM21 was undistinguishable from TRV130, a G_i-biased opioid agonist now in Phase III clinical trials (Fig. 3f, g), whereas its G-protein-bias substantially exceeded that of herkinorin, which has also been purported to be a G_i-biased agonist[33] (Extended Data Fig. 6). An intriguing distinction in these signalling studies is the lack of agonist activity of PZM21 at κOR. While PZM21 is an 18-nM antagonist of this receptor, the other biased agonist, TRV130, activates κOR with similar potency to morphine (Extended Data Fig. 6f). Additionally, despite having similar levels of signalling bias, in modelling studies TRV130 and PZM21 appear to engage the µOR in distinct ways (Extended Data Fig. 2f).

Analgesia with diminished side effects

Consistent with its µOR agonist activity, PZM21 displayed dose-dependent analgesia in a mouse hotplate assay, with a per cent maximal possible effect (% MPE) of 87% reached 15 min after administration of the highest dose of drug tested (Fig. 4a). The highest dose of morphine tested plateaued at 92% after 30 min. Intriguingly, we observed no analgesic effect for PZM21 in the tail-flick assay (Fig. 4b). Such a distinction is unprecedented among opioid analgesics. The hotplate experiment assesses analgesia at both higher-level central nervous system (CNS) brain and spinal nociceptive circuits, while the tail-flick experiment is more specific for spinal reflexive responses[34]. Subcategorizing the behavioural responses in the hotplate experiment as either affective (CNS mediated) or reflexive (spinally

mediated) showed that, unlike morphine, PZM21 solely confers analgesia to the affective component of pain (Fig. 4c and Extended Data Fig. 7a, b). Though separation of these two analgesic pathways is unique to PZM21 among known opioid analgesics, it has been observed by selective chemogenetic activation[35] or toxin-induced inactivation of CNS neurons in rodents[36]. Indeed, PZM21 is also active in a formalin injection nociception assay, likely from supraspinal activation of descending inhibitory circuits[37] (Fig. 4d). Whether this circuit-specificity reflects the biased signalling of PZM21, its specificity for the µOR versus other opioid receptors and other GPCRs, an unusual CNS distribution phenomenon, or some other signalling property, is uncertain at this time. More certain is that PZM21 analgesia results from µOR activation *in vivo* as genetic knockout of the µOR completely ablates the observed analgesic response in the hotplate assay (Fig. 4e). Meanwhile, PZM21 is metabolized relatively slowly by mouse liver microsomes, with only 8% metabolism over one hour. Signalling experiments with the resulting metabolite pool show no evidence of a metabolite with more potent activation of the µOR, confirming that the observed analgesic activity results primarily from the originally administered dose of PZM21 (Extended Data Fig. 7e, f).

Based on previous genetic studies with arrestin knockout mice and pharmacological studies with biased compounds[4–7], we anticipated that PZM21 would confer longer-lasting analgesia with decreased respiratory depression and constipation—both key dose-limiting side-effects of classic opioid agonists. Analgesia induced by PZM21 lasts up to 180 min, substantially longer than that induced by a maximal dose of morphine (Extended Data Fig. 7a, b) and the biased agonist TRV130 (Fig. 4a). Whereas PZM21 does reduce defecation, its constipating effect is substantially less than morphine (Fig. 4f). Respiratory depression was investigated by dosing unrestrained mice with equi-analgesic doses of PZM21, TRV130 and morphine (40 mg kg^{-1}, 1.2 mg kg^{-1}, and 10 mg kg^{-1}, respectively), and measuring respiration by whole-body plethysmography. While morphine profoundly depressed respiration frequency, PZM21 was almost undistinguishable from vehicle (Fig. 4g). By comparison, TRV130 significantly depresses respiration at 15 min, correlating with its peak analgesic response. Although respiratory depression by µOR may be partially mediated by activation of G-protein-coupled inwardly rectifying potassium channels (GIRKs), systemically infused opioids can decrease respiratory frequency even in GIRK-deficient mice[38], consistent with the G-protein-independent signalling mechanisms first suggested by the arrestin knockout studies[4–6]. The rapid respiratory depression observed for morphine and TRV130 may reflect GIRK activation. At later time points, however, PZM21 induces minimal respiratory depression despite providing robust analgesia. Conversely, morphine induces a prolonged course of respiratory depression that does not subside with resolution of the analgesic response at 90 min. This dissociation in analgesia and respiratory depression at later time points may reflect differential recruitment of β-arrestin-2. Taken together, these studies support minima l β-arrestin-2 signalling *in vivo* by PZM21 (biased signalling, Fig. 1a).

A major liability of current opioid analgesics is reinforcement and addiction, which are both postulated to be mediated—at least in part—by activation of the dopaminergic reward circuits[39]. A biomarker for such activation in mice is an acute hyperlocomotive response, reflecting mesolimbic dopaminergic activation[40]. Whereas morphine induced mouse

hyperlocomotion in an open-field assay (Fig. 4h), a nearly equi-analgesic dose of PZM21 had no apparent effect on locomotion versus vehicle. The decreased distance travelled does not reflect a cataleptic effect of PZM21 (Extended Data Fig. 7c). Consistent with decreased activation of reward circuits, administration of PZM21 also does not induce a conditioned place preference response (Fig. 4i), unlike morphine and other opioids[41]. Though TRV130 does trend more towards inducing place preference, its activity is also not significant relative to vehicle; this lack of conditioned place preference for both biased agonists may support a role for G-protein bias in the lack of opioid-induced reinforcing behaviour. The differences between morphine and PZM21 in conditioned place preference do not simply reflect dissimilarities in CNS penetration between the two drugs, as a substantial fraction of PZM21 crosses the blood–brain barrier (Extended Data Fig. 7d).

Several caveats deserve to be mentioned. Although structure-based discovery succeeded in finding novel scaffolds and supported facile optimization, some of the properties of PZM21 were likely fortuitous. Biased signalling through G protein and arrestin pathways reflects the stabilization of conformations over 30 Å from the orthosteric site where PZM21 binds. We did not select molecules that preferentially stabilize these conformations, but instead relied on chemical novelty to confer new biological properties. Receptor subtype selectivity was attained by simply selecting molecules that extended into variable regions of the receptor, a strategy that may not always work. Several aspects of the pharmacology presented here remain preliminary, including the metabolic stability studies and the pharmacokinetics, and it is not clear at this time whether the unprecedented *in vivo* activity of PZM21 reflects its biased and specific agonism, or some other feature conferred by its novel chemotype. Finally, identification of agonists from docking to an inactive state receptor structure cannot always be relied upon[13,16,42,43], though there is precedence for doing so against opioid receptors[23].

Discussion

Notwithstanding these caveats, this study supports a structure-based approach for GPCR ligand discovery. Whereas this method cannot yet reliably find leads with tailored specificity and signalling efficacy, it can reliably identify entirely new scaffolds and chemotypes. These new chemotypes may stabilize receptor conformations not explored previously and so generate novel biological effects. With a novel chemotype in hand, the docked structure provides a straight-forward strategy for optimization. Here, we optimized an initial docking hit, compound **7**, 1,000-fold to the final lead molecule, PZM21, by evaluating fewer than 50 molecules. Though this campaign was inspired by existing μOR-biased agonists like TRV130[7], the structure-based approach led to a compound with novel properties; it was structurally distinct compared to previously explored opioid ligands, with not only substantial signalling bias but also with unexpected opioid receptor selectivity. These features have contributed to favourable biological effects, with long-lasting analgesia coupled to apparent elimination of respiratory depression, specificity for central over reflex analgesia, lack of locomotor potentiation and conditioned place preference, and hence a reduced potential for opioid-induced reinforcement for PZM21 and molecules like it. The selectivity, potency, and biased signalling of PZM21 make it a tool molecule of a sort previously unavailable to interrogate μOR signalling. More broadly, the *in vitro* results of

multiple GPCR campaigns, and the *in vivo* results reported here, portend a general approach to the problem of new tool and lead discovery for this pharmacologically important family of receptors.

METHODS

No statistical methods were used to predetermine sample size.

Chemicals, reagents, and cell lines

Chemicals and reagents used in this study were purchased from commercial sources (Sigma, Tocris, Fisher scientific, ZINC database suppliers) or synthesized as outlined in the Supplementary Information. HEK293 (ATCC CRL-1573; 60113019; certified mycoplasma free and authentic by ATCC) and HEK293-T (HEK293T; ATCC CRL-11268; 59587035; certified mycoplasma free and authentic by ATCC) cells were from the ATCC and are well validated for signalling studies. Cells were also validated by analysis of short tandem repeat (STR) DNA profiles and these profiles showed 100% match at the STR database from ATCC. U2OS cells expressing human μOR were obtained as cryopreserved stocks from DiscoverX and were not further authenticated.

Molecular docking and analogue selection

The inactive-state μ-opioid receptor structure (PDB: 4DKL) was used as input for receptor preparation with DOCK Blaster (http://blaster.docking.org)[44]. Forty-five matching spheres were used based on a truncated version of the crystallized ligand. The covalent bond and linker region of the antagonist β-funaltrexamine were removed for sphere generation. The ligand sampling parameters were set with bin size, bin size overlap, and distance tolerances of 0.4 Å, 0.1 Å, and 1.5 Å, respectively, for both the matching spheres and for the docked molecules. Ligand poses were scored by summing the receptor-ligand electrostatics and van der Waals interaction energy corrected for ligand desolvation. Receptor atom partial chargers were used from the united atom AMBER force field except for Lys233 and Tyr326, where the dipole moment was increased as previously described[43]. Over 3 million commercially available molecules from the ZINC[20] (http://zinc.docking.org) lead-like set were docked into the receptor using DOCK3.6[21] (http://dock.compbio.ucsf.edu). Among the top ranking 0.08% of molecules were inspected and 23 were selected for experimental testing in the primary screen. A resource to perform these docking studies is publicly available (http://blaster.docking.org).

For a secondary screen, analogues of the top three hits from the primary screen (compounds **4**, **5** and **7**) with a similarity of greater than 0.7 (as defined in the ZINC search facility) were identified in the ZINC database. Additionally, substructure searches were performed using the scaffolds of each of these three compounds. The searches yielded 500 purchasable compounds, which were then docked as in the primary screen. Analogues were manually inspected for interactions and selected for further experimental testing.

Radioligand binding studies

For a primary screen of selected molecules, binding to μOR was assessed by measuring competition against the radioligand ^{3}H-diprenorphine (^{3}H-DPN). Each compound was initially tested at 20 μM and was incubated with ^{3}H-DPN at a concentration equal to the K_d (0.4 nM) of the radioligand in μOR containing *Sf9* insect cell membranes. The reaction contained 40 fmol of μOR and was incubated in a buffer of 20 mM HEPES pH 7.5, 100 mM sodium chloride, and 0.1% bovine serum albumin for 1 h at 25 °C. To separate free from bound radioligand, reactions were rapidly filtered over Whatman GF/B filters with the aid of a Brandel harvester and ^{3}H-DPN counts were measured by liquid scintillation. Compounds with more than 25% of ^{3}H-DPN radioactivity were further tested in full dose–response to determine the affinity (K_i) in HEK293 membranes. Subsequently, the 15 analogues were tested in full dose–response for affinity at the μOR and the κOR by the National Institutes of Mental Health Psychoactive Drug Screen Program (PDSP)[45], as were the affinities of compounds **12**, PZM21, and their stereoisomers at the μOR, δOR, κOR and nociception receptor.

Radioligand depletion assays to test the irreversible binding of compound PZM29 were performed as described previously[46]. Human embryonic kidney 293 (HEK 293) cells were transiently transfected with μOR or the cysteine mutant μOR:N127C using the Mirus TransIT-293 transfection reagent (MoBiTec, Goettingen, Germany), grown for 48 h, harvested, and homogenates were prepared as described[47]. For radioligand depletion experiments, homogenates were preincubated in TRIS buffer (50 mM Tris at pH 7.4) at a protein concentration of 50–100 μg/ml or 70–120 μg/ml for μOR and μOR:N127C, respectively and the covalent ligand (at 5 μM) for different time intervals. Incubation was stopped by centrifugation and reversibly bound ligand was washed three times (resuspension in buffer for 30 min and subsequent centrifugation). Membranes were then used for radioligand binding experiments with ^{3}H-diprenorphine (final concentration: 0.7 nM, specific activity: 30 Ci/mmol, purchased from Biotrend, Cologne, Germany) to determine specific binding at the μOR (B_{max} = 4,000–6,500 fmol/mg protein, K_D = 0.25–0.45 nM) and the μOR:N127C receptor (B_{max} = 1,300–6,000 fmol/mg protein, K_D = 0.18–0.25 nM), respectively as described[48]. Non-specific binding was determined in the presence of 10 μM naloxone. For data analysis, the radioactivity counts were normalized to values where 100% represents effect of buffer and 0% represents non-specific binding. Five independent experiments, each done in quadruplicate, were performed and the resulting values were calculated and pooled to a mean curve which is displayed.

GTP-γS Binding Experiments

The [^{35}S]-GTPγS binding assay was performed with membrane preparations from HEK 293 cells coexpressing the human μOR and the PTX insensitive G-protein subunits $G_{\alpha o1}$ or $G_{\alpha i2}$[49]. Cells were transiently transfected using the Mirus TransIT-293 transfection reagent (MoBiTec, Goettingen, Germany), grown for 48 h, harvested and homogenates were prepared as described[47]. The receptor expression level (B_{max}) and K_D values were determined in saturation experiments with ^{3}H-diprenorphine (specific activity: 30 Ci/mmol, purchased from Biotrend, Cologne, Germany) (B_{max} = 3,700 ± 980 fmol/mg protein, K_D = 0.30 ± 0.093 nM for μOR+ $G_{\alpha o1}$ or B_{max} = 5,800 ± 2,000 fmol/mg, K_D = 0.46 ± 0.095 nM

for µOR+ $G_{\alpha i2}$, respectively). The assay was carried out in 96-well plates with a final volume of 200 µl. In each well, 10 µM GDP, the compounds (0.1 pM to 100 µM final concentration) and the membranes (30 µg/ml final protein concentration) were incubated for 30 min at 37 °C in incubation buffer containing 20 mM HEPES, 10 mM $MgCl_2 \cdot 6 H_2O$ and 70 mg/l saponin. After the addition of 0.1 nM [^{35}S] -GTPγS (specific activity 1,250 Ci/mmol, PerkinElmer, Rodgau, Germany) incubation was continued at 37 °C for further 30 min or 75 min for µOR+ $G_{\alpha o1}$ or µOR+ $G_{\alpha i2}$, respectively. Incubation was stopped by filtration through Whatman GF/B filters soaked with ice cold PBS. Bound radioactivity was measured by scintillation measurement as described previously[48].

Data analysis was performed by normalizing the radioactivity counts (ccpms) to values when 0% represents the non-stimulated receptor and 100% the maximum effect of morphine or DAMGO. Dose–response curves were calculated by nonlinear regression in GraphPad Prism 6.0. Mean values ± s.e.m. for EC_{50} and E_{max} values were derived from 3–12 individual experiments each done in triplicate.

$G_{i/o}$ induced cAMP inhibition

To measure µOR $G_{i/o}$-mediated cAMP inhibition, HEK-293T cells were co-transfected using calcium phosphate in a 1:1 ratio with human µOR and a split-luciferase based cAMP biosensor (pGloSensor™-22F; Promega). For experiments including GRK2 co-expression, cells were transfected with 1 µg/15-cm dish of GRK2. After at least 24 h, transfected cells were washed with phosphate buffered saline (PBS) and trypsin was used to dissociate the cells. Cells were centrifuged, resuspended in plating media (1% dialysed FBS in DMEM), plated at a density of 15,000–20,000 cells per 40 µl per well in poly-lysine coated 384-well white clear bottom cell culture plates, and incubated at 37 °C with 5% CO_2 overnight. For inactivation of pertussis-toxin (PTX) $G_{\alpha i/o}$ experiments, cells were plated with 100 ng/ml final concentration PTX. The next day, drug dilutions were prepared in fresh assay buffer (20 mM HEPES, 1 × HBSS, 0.1% bovine serum album (BSA), and 0.01% ascorbic acid, pH 7.4) at 3 × drug concentration. Plates were decanted and 20 µl per well of drug buffer (20 mM HEPES, 1× HBSS, pH 7.4) was added to each well. Drug addition to 384-well plates was performed by FLIPR adding 10 µl of drug per well for a total volume of 30 µl. Plates were allowed to incubate for exactly 15 min in the dark at room temperature. To stimulate endogenous cAMP via β adrenergic-G_s activation, 10 µl of 4 × isoproterenol (200 nM final concentration) diluted in drug buffer supplemented with GloSensor assay substrate was added per well. Cells were again incubated in the dark at room temperature for 15 min, and luminescence intensity was quantified using a Wallac TriLux microbeta (Perkin Elmer) luminescence counter. Data were normalized to DAMGO-induced cAMP inhibition and analysed using nonlinear regression in GraphPad Prism 6.0 (Graphpad Software Inc., San Diego, CA).

Determination of functional activity of PZM21-29 for SAR studies was performed using a BRET-based cAMP accumulation assay[50]. HEK-293T cells were transiently co-transfected with pcDNA3L-His-CAMYEL42 (purchased from ATCC via LCG Standards, Wesel, Germany) and human µOR, achieving a cDNA ratio of 2:2 using Mirus TransIT-293 transfection reagent. 24 h post-transfection, cells were seeded into white half-area 96-well

plates at 20×10^4 cells/well and grown overnight. On the following day, phenol-red-free medium was removed and replaced by PBS and cells were serum starved for 1 h before treatment. The assay was started by adding 10 µl coelenterazine h (Progmega, Mannheim, Germany) to each well to yield a final concentration of 5 µM. After 5 min incubation, compounds were added in PBS containing forskolin (final concentration 10 µM). Reads of the plates started 15 min after agonist addition. BRET readings were collected using a CLARIOstar plate reader (BMG LabTech, Ortenberg, Germany). Emission signals from Renilla Luciferase and YFP were measured simultaneously using a BRET1 filter set (475-30 nm/535-30 nm). BRET ratios (emission at 535-30 nm/emission at 475-30 nm) were calculated and dose–response curves were fitted by nonlinear regression using GraphPad Prism 6.0. Curves were normalized to basal BRET ratio obtained from dPBS and the maximum effect of morphine and DAMGO. Each curve is derived from three to five independent experiments each done in duplicate.

Calcium release

Calcium release was measured using a FLIPR^{TETRA} fluorescence imaging plate reader (Molecular Devices). Calcium release experiments were run in parallel to $G_{i/o}$ Glosensor experiments with the same HEK-293T cells transfected with µOR, except cells for FLIPR were plated in poly-lysine coated 384-well black clear bottom cell culture plates. Cells were incubated at 37 °C with 5% CO_2 overnight and next day media was decanted and replaced with Fluo-4 direct calcium dye (Life Technologies) made up in HBSS with 20 mM HEPES, pH 7.4. Dye was incubated for 1 h at 37 °C. Afterwards, cells were equilibrated to room temperature, and fluorescence in each well was read for the initial 10 s to establish a baseline. Afterwards, 10 µl of drug (3×) was added per well and the maximum-fold increase in fluorescence was determined as fold-over-baseline. Drug solutions used for the FLIPR assay were exactly the same as used for $G_{i/o}$ Glosensor experiments. To activate endogenous G_q-coupled receptors as a positive control for calcium release, TFLLR-NH$_2$ (10µM, PAR-1 selective agonist) was used.

Receptor internalization

Internalization was measured using the eXpress DiscoveRx PathHunter GPCR internalization assay using split β-galactosidase complementation. In brief, cryopreserved U2OS cells expressing the human µOR were thawed rapidly and plated in supplied medium and 96-well culture plates. Next day, cells were stimulated with drugs (10×) and allowed to incubate for 90 min at 37 °C with 5% CO_2. Afterwards, substrate was added to cells and chemiluminescence was measured on a TriLux (Perkin Elmer) plate counter. Data were normalized to DAMGO and analysed using Graphpad Prism 6.0.

β-Arrestin recruitment assays

β-Arrestin recruitment was measured by either the PathHunter enzyme complementation assay (DiscoveRx) or by previously described bioluminescence resonance energy transfer (BRET) methods[51]. Assays using DiscoveRx PathHunter eXpress OPRM1 CHO-K1 β-Arrestin GPCR Assays were conducted exactly as instructed by the manufacturer. Briefly, supplied cryopreserved cells were thawed and resuspended in the supplied medium, and plated in the furnished 96-well plates. Next day, 10× dilutions of agonist (prepared in HBSS

and 20 mM HEPES, pH 7.4) were added to the cells and incubated for 90 min. Next, the detection reagents were reconstituted, mixed at the appropriate ratio, and added to the cells. After 60 min, luminescence per well was measured on a TriLux (Perkin-Elmer) plate counter. Data were normalized to DAMGO and analysed using the sigmoidal dose–response function built into GraphPad Prism 6.0.

To measure μOR mediated β-arrestin recruitment by BRET in the presence or absence of GRK2 co-expression, HEK-293T cells were co-transfected in a 1:1:15 ratio with human μOR containing C-terminal *renilla* luciferase (*R*Luc8), GRK2, and venus-tagged N-terminal β-arrestin-2, respectively. In the case of experiments where GRK2 expression was varied, pcDNA3.1 was substituted for GRK2 to maintain the same concentration of DNA transfected. After at least 24 h, transfected cells were plated in poly-lysine coated 96-well white clear bottom cell culture plates in plating media at a density of 125,000–250,000 cells per 200 μl per well and incubated overnight. The next day, media was decanted and cells were washed twice with 60 μl of drug buffer and incubated at room temperature for at least 10 min before drug stimulation. 30 μl of drug (3×) was added per well and incubated for at least 30 min in the dark. Then, 10 μl of the *R*Luc substrate, coelenterazine H (Promega, 5 μM final concentration) was added per well, and plates were read for both luminescence at 485 nm and fluorescent eYFP emission at 530 nm for 1 s per well using a Mithras LB940 microplate reader. The ratio of eYFP/*R*Luc was calculated per well and the net BRET ratio was calculated by substracting the eYFP/*R*Luc per well from the eYFP/*R*Luc ratio without venus–arrestin present. Data were normalized to DAMGO-induced stimulation and analysed using nonlinear regression in GraphPad Prism 6.0.

Ligand bias calculation

Multiple approaches have been described to quantitate ligand bias, including operational models, intrinsic relative activity models, and allosteric models[31,52]. In the absence of GRK2, we observe no β-arrestin-2 recruitment for PZM21 and TRV130. This prevents a quantitative assessment of bias by the operational model. In the case where GRK2 is overexpressed, we observe arrestin recruitment for PZM21 and TRV130. In this case, we utilize the operational model to calculate ligand bias and display equiactive bias plots for comparison of ligand efficacy for distinct signalling pathways[31,53]. The Glosensor $G_{i/o}$, DiscoverX PathHunter β-arrestin, or net BRET concentration response curves were fit to the Black-Leff operational model to determine transduction coefficients (τ/K_A). Compound bias factors are expressed after normalization against the prototypical opioid agonist DAMGO used as a reference. Bias factors are expressed as the value of $\log[\tau/K_A]$.

Assessment of off-target PZM21 activity

To identify potential off-target activity of PZM21, we used the National Institutes of Mental Health Psychoactive Drug Screen Program. Compound PZM21 was first tested for activity against 320 non-olfactory GPCRs using the PRESTO-Tango GPCRome screening β-arrestin recruitment assay[30]. We used 10 μM PZM21 and activity at each receptor was measured in quadruplicate. Potential positive receptor hits were defined as those that increase the relative luminescence value twofold. Positive hits were subsequently re-tested in full dose–response mode to determine whether the luminescence signal titrates with increasing concentrations

of PZM21. A number of false-positive hits were discounted by this approach. PZM21 inhibition of hERG channel was performed as described previously[54] and neurotransmitter transporter assays were determined used the Molecular Devices Neurotransmitter Assay Kit (Molecular Devices).

In vivo studies

Adult male C57BL/6J (aged 3–5 months) obtained from Jackson Laboratories (Bar Harbour, Maine) were used to investigate behavioural responses, respiratory effects, and hyperlocomotion induced by PZM21 and compared with morphine or vehicle (0.9% sodium chloride). For μOR knockout animals, *Oprm1*$^{-/-}$ mice (B6.129S2-Oprm1tm1Kff/J) were obtained from Jackson Laboratories. All drugs were dissolved in vehicle and injected subcutaneously Behavioural studies were conducted at the University of North Carolina and Stanford University following the National Institutes of Health's guidelines for care and use of animals and with approved mouse protocols from the institutional animal care and use committees. Sample sizes (number of animals) were not predetermined by a statistical method and animals were assigned to groups randomly. Drug treatment groups were only blinded for measurement of affective versus reflexive analgesia; other experiments were not blinded to investigators. Predefined exclusion criteria were set for analgesia and conditioned preference experiments. No animals were excluded from statistical analysis. Statistical analyses were performed after first assessing the normality of distributions of data sets and Leven's test was used to assess equality of variances.

Measurement of analgesia

Analgesia-like responses in were measured as previously described[55] using a hotplate analgesia meter with dimensions of 29.2×26.7 cm with mice restricted to a cylinder 8.9 cm in diameter and 15.2 cm high (IITC Life Sciences, Woodland Hills, California). Response was measured by recording the latency to lick, flutter, or splay hind paw(s), or an attempt to jump out of the apparatus at 55 °C, with a maximum cut-off time of 30 s. Once a response was observed or the cut-off time had elapsed, the subject was immediately removed from the hotplate and placed back in its home cage. The animals were acclimated to the hotplate, while cool, and a baseline analgesic response time was acquired several hours before drug treatment and testing. Mice were injected with either vehicle ($n = 8$), morphine (5 mg/kg, $n = 8$ or 10 mg/kg, $n = 8$), TRV130 (1.2 mg/kg, $n = 9$) or PZM21 (10 mg/kg, $n = 8$; 20 mg/kg, $n = 11$; or 40 mg/kg, $n = 8$). After injection of drug, the analgesic effect expressed as percentage maximum possible effect (%MPE) was measured at 15, 30, 60, 90 and 120 min after drug treatment. If animals did not display hind paw lick, splay, or flutter, they were removed from the trial. Additionally, if animals attempted to jump out of the plate or urinated on the hotplate they were removed from the trial. To assess analgesia by the tail-flick assay, a tail-flick analgesia meter (Columbus Instruments, Columbus, Ohio). Mice were gently immobilized with a cotton towel and the tail base was placed on a radiant light source emitting a constant temperature of 56 °C. The tail withdrawal latency was measured at similar time points as the hotplate assay after administration of vehicle ($n = 8$), morphine (5 mg/kg, $n = 4$; 10 mg/kg, $n = 8$) or PZM21 (10 mg/kg, $n = 8$; 20 mg/kg; $n = 14$). The cut-off time for the heat source was set at 10 s to avoid tissue damage. Analgesic response times were measured similar to the hotplate assay.

Analgesia in μOR knockout mice and subcategorization of affective/reflexive pain

Oprm1⁻/⁻ and wild-type C57Bl/6J mice (male; 8–11 weeks) were acclimated to the testing environment and thermal-plate equipment for three non-consecutive days between 11:00 and 13:00 before any pharmacological studies. Acclimation was achieved by individually confining mice within an enclosed semi-transparent red plastic cylinder (10 cm depth × 15 cm height) on a raised metal-mesh rack (61 cm height) for 30 min, and then exposing each mouse to the thermal-plate equipment (non-heated; floor dimensions, 16.5 × 16.5 cm; Bioseb), while confined within a clear plastic chamber (16 cm length × 16 cm width × 30 cm height). Acclimation exposure to the thermal plate lasted for 30 s, and exposure was repeated after 30 min to mimic the test day conditions. The testing environment had an average ambient temperature of 22.6 °C and illumination of 309 lx from overhead fluorescence lighting. The same male experimenter (G.C.) was present throughout the entire duration of habituation and testing to exclude possible olfaction-induced alterations in sensory thresholds[56].

Cutaneous application of a noxious stimulus, or time spent on a hotplate apparatus can broadly elicit several distinct behavioural responses: 1) withdrawal reflexes: rapid reflexive retraction or digit splaying of the paw; 2) affective-motivational responses: directed licking and biting of the paw, and/or a motivational response characterized by jumping away from the heated floor plate. Paw withdrawal reflexes are classically measured in studies of hypersensitivity, and involve simple spinal cord and brainstem circuits[57]. In contrast, affective responses are complex, non-stereotyped behaviours requiring processing by limbic and cortical circuits in the brain, the appearance of which indicates the subject's motivation and arousal to make the unpleasant sensation cease by licking the affected tissue, or seeking an escape route[36],[57–64]. To distinguish between potential differential analgesic effects of PZM21, mice were placed on the heated apparatus (52.5 °C), and the latency to exhibition of the first sign of a hindpaw reflexive withdraw, and the first sign of an affective response was recorded. A maximum exposure cut-off of 30 s was set to reduce tissue damage. Mice were injected with either vehicle ($n = 6$), morphine (10 mg/kg, $n = 10$), or PZM21 (20 mg/kg, $n = 13$). After injection of drug, the analgesic effect on either reflex or attending responses was expressed as percentage maximum possible effect (%MPE), and was measured at − 30 (baseline), 15, 30, 60, 90, 120, and 180 min relative to drug treatment. For studies comparing *Oprm1⁻/⁻* and wild-type C57Bl/6J mice, the analgesic response in the hotplate assay was measured 30 min after injection of vehicle ($n = 5$ for both genotypes), morphine (10 mg/kg, $n = 5$ for both genotypes) or PZM21 (20 mg/kg, $n = 6$ for *Oprm1⁻/⁻* and $n = 5$ for wild-type).

Formalin injection assay

Analgesia to formalin injection was carried out as described previously[65]. Mice were first habituated for 20 min to the testing environment which included a home cage without bedding, food, and water. After habituation, vehicle ($n = 6$), morphine (10 mg/kg, $n = 7$), or PZM21 (40 mg/kg, $n = 7$) was injected subcutaneously. This was followed by injection of 20 μl of 1% formalin in 0.9% saline under the skin of the dorsal surface of the right hindpaw. Animals were returned to their home cage and behavioural responses were recorded for one hour. Nociception was estimated by measuring the cumulative time spent by animals licking

the formalin-injected paw. As opioids classically display two phases of analgesic action, nociceptive behaviour was measured during both the early phase (0 to 5 min) and the late phase (20 to 30 min). In Fig. 4, an asterisk indicates a significant difference between drug and vehicle ($P < 0.05$ calculated using a one-way ANOVA with Bonferroni correction).

Mouse plethysmography

Respiration data was collected using a whole body plethysmography system (Buxco Electronics Inc., Wilmington, North Carolina) as described[66]. This method measures respiratory frequency, tidal volume, peak flows, inspiratory time, and expiratory time in conscious and unrestrained mice. Briefly, Buxco airflow transducers were attached to each plethysmography chamber and a constant flow rate was maintained for all chambers. Each chamber was calibrated to its attached transducer before the experiment. Animals were first habituated to the clear plexiglass chambers for 10 min. Respiratory parameters were recorded for 10 min to establish a baseline before injection of vehicle ($n = 8$), morphine (10 mg/kg, $n = 8$), TRV130 (1.2 mg/kg, $n = 8$) or PZM21 (40 mg/kg, $n = 8$). Respiratory parameters were then collected on unrestrained mice for 100 min post drug injection. To decrease respiratory variability induced by anxiety, mice were shielded from view of other animals and experimenter. In Fig. 4, an asterisk indicates a significant difference between drug and vehicle ($P < 0.05$ calculated using a repeated measures ANOVA with Bonferroni correction).

Accumulated faecal boli quantification

To measure constipatory effects of morphine and PZM21, we assessed the total accumulated faecal boli as described[6]. Briefly, mice were injected with vehicle ($n = 10$), morphine (10 mg/kg, $n = 16$) or PZM21 (20 mg/kg, $n = 16$) and placed within a plexiglass chamber (5 cm × 8 cm × 8 cm) positioned on a mesh screen. Mice were maintained without food or water for 6 h. Faecal boli were collected underneath the mesh on a paper towel and the cumulative mass was measured every hour for six hours. In Fig. 4, an asterisk indicates a significant difference between drug and vehicle ($P < 0.05$ calculated using a repeated measures ANOVA with Bonferroni correction).

Open field locomotor response

A photocell-equipped automated open field chamber (40 cm × 40 cm × 30 cm; Versamax system, Accuscan Instruments) contained inside sound-attenuating boxes was used to assess locomotor activity. Baseline ambulation of freely moving mice was monitored over 30 min, followed by injection with vehicle ($n = 7$), morphine (10 mg/kg, $n = 5$) or PZM21 (20 mg/kg, $n = 6$). Locomotor activity was monitored for another 150 min. In Fig. 4, an asterisk indicates a significant difference between drug and vehicle ($P < 0.05$ calculated using a repeated measures ANOVA with Bonferroni correction).

Conditioned place preference

A three-chambered conditioned place preference apparatus (Med-Associates, St. Albans, Vermont) consisting of white or black chambers (16.8 × 12.7 × 12.7 cm each) with uniquely textured white mesh or black rod floors and separated by a neutral central chamber (7.2 ×

12.7 × 12.7 cm) was used for conditioned place preference testing. On day 1 (preconditioning day), mice were placed in the central chamber and allowed to explore freely for 30 min. Time spent in each compartment was used to estimate baseline chamber preferences and mice showing specific chamber bias more than 70% were not studied further. On days 2–9 (conditioning days) mice were injected with either vehicle or drug and paired with either the white mesh or the black rod chambers. All mice received vehicle on days 2, 4, 6, 8 and drug on days 3, 5, 7, 9. On day 10 (test day), mice were again placed in the central chamber as on day 1 and allowed to explore freely for 30 min. Time spent in each chamber was expressed as percentage preference. Place preference was tested with morphine (10 mg/kg, $n = 16$), PZM21 (20 mg/kg, $n = 8$), or TRV130 (1.2 mg/kg, $n = 7$). In Fig. 4, an asterisk indicates a significant difference between vehicle and drug chambers ($P < 0.05$ by one-sample t-test with hypothetical value of 50) while NS indicates non-significance ($P > 0.05$).

Cataleptic effect

Drug induced catalepsy was measured in mice using the bar test[67], which includes a horizontally placed 3-mm diameter wooden bar fixed 4 cm above the floor. Mice were habituated with the bar and the environment for 20 min before subcutaneous injection of either haloperidol (2 mg/kg, $n = 8$), morphine (10 mg/kg, $n = 8$), or PZM21 (20 mg/kg, $n = 8$). To measure catalepsy, both forepaws were gently placed on the bar and the length of time during which each mouse remained in the initial position was measured. The effect was measured at 15, 30 and 90 min after drug injection. Maximum cut-off time for each challenge was 90 s.

Pharmacokinetics of PZM21

Studies were performed by the Preclinical Therapeutics Core and the Drug Studies Unit at the University of California San Francisco. Ten mice were injected subcutaneously with 20 mg/kg of PZM21. At each time point, 1 ml of blood was collected from three mice and the serum concentration of PZM21 determined by liquid chromatography–mass spectrometry (LC/MS). Mice were subsequently sacrificed and entire brains were homogenized for determination of PZM21 concentrations by LC/MS. All studies were performed with approved mouse protocols from the institutional animal care and use committees.

Metabolism of PZM21

Metabolism experiments were performed as described previously[68]. In brief, pooled microsomes from male mouse liver (CD-1) were purchased (Sigma Aldrich) and stored at −75 °C until required. NADPH was purchased (Carl Roth) and stored at −8 °C. The incubation reactions were carried out in polyethylene caps (Eppendorf 1.5 ml) at 37 °C. The incubation mixture contained PZM21 (80 μM) or positive controls (imipramine and rotigotine), pooled liver microsomes (0.5 mg of microsomal protein/ml of incubation mixture) and Tris-MgCl$_2$ buffer (48 mM Tris, 4.8 mM MgCl$_2$, pH 7.4). The final incubation volume was 0.5 ml. Microsomal reactions were initiated by addition of 50 μl of enzyme cofactor solution NADPH (final concentration of 1 mM). At 0, 15, 30 and 60 min the enzymatic reactions were terminated by addition of 500 μl of ice-cold acetonitrile (containing 8 μM internal standard), and precipitated protein was removed by centrifugation

(15,000 rcf for 3 min). The supernatant was analysed by HPLC/MS (binary solvent system, eluent acetonitrile in 0.1% aqueous formic acid, 10–40% acetonitrile in 8 min, 40–95% acetonitrile in 1 min, 95% acetonitrile for 1 min, flow rate of 0.3 ml/min). The experiments were repeated in three independent experiments. Parallel control incubations were conducted in the absence of cofactor solution to determine unspecific binding to matrix. Substrate remaining and metabolite formation was calculated as a mean value ± s.e.m. of three independent experiments by comparing AUC of metabolites and substrate after predetermined incubation time to AUC of substrate at time 0, estimating a similar ionization rate, corrected by a factor calculated from the AUC of internal standard at each time point.

Chemical synthesis

The stereochemically pure isomers of **12** and PZM21 were synthesized from corresponding (*R*)- and (*S*)-amino acid amides, which were either commercially available or readily prepared from the corresponding acid or ester (see Supplementary Information). The primary amino group was dimethylated using an excess of aqueous formaldehyde and sodium triacetoxyborohydride in aqueous acetonitrile. The carboxamides **16a,b** were converted to primary amines by treatment with borane-tetrahydrofurane complex under reflux yielding the diamines **17a,b**. Henry reaction of thiophene-3-carbaldehyde with nitroethane afforded the nitropropene derivative **18**, which was converted into the racemic alkylamine **19**. Activation with 4-nitrophenyl chloroformate yielded the carbamates **20**, which were coupled with the enantiopure primary amines **17a,b** to achieve diastereomeric mixtures of the corresponding ureas **12** and **21**. HPLC separation using a semi-preparative Chiralpak AS-H column gave the overall eight pure stereoisomers of **12** and **21** including PZM21.

To determine the absolute configuration of the final products and efficiently prepare PZM21, we synthesized enantiomerically enriched carbamate **20**, coupled it with the corresponding primary amines. For enantiomeric enrichment, we performed chiral resolution of the racemic primary amine **19** via repetitive crystallization with di-p-anisoyl-(*S*)-tartaric acid. After triple crystallization, we obtained **19** enriched in dextrorotatory enantiomer ($[\alpha]_D^{25} = + 20.5°$). The corresponding (*R*)-acetamide has been previously characterized as dextrorotatory ($[\alpha]_D^{20} = + 49.8°$), so enantiomerically enriched **19** was treated with acetic anhydride and triethylamine, and the specific rotation of the product was measured. Based on the value of specific rotation of the resulting acetamide ($[\alpha]_D^{21} = - 46.6°$), we assigned the absolute configuration of the major isomer to be (*S*). (*S*)-enriched **20** was used for synthesis of the final urea derivatives and absolute configuration of diastereomers in pairs was assigned based on the equality of retention time in chiral HPLC. A full description of the synthetic routes and analytical data of the compounds **12**, PZM21 and its analogues PZM22-29 are presented in the Supplementary Information.

Detailed modelling of PZM21 and TRV130 binding poses

PZM21 was docked to the inactive state μOR structure using DOCK3.6 (ref 21) as described for the primary screen, with the exception that the 45 matching spheres used were generated based on the docked pose of compound **12**. The resulting ligand-receptor complex was further optimized through minimization with the AMBER protein force field[69] and the

GAFF ligand force field supplemented with AM1-BCC charges. Docking of PZM21 and TRV130 to the active state μOR structure (PDB: 5C1M) was also performed with DOCK3.6 with parameters as described above. The amino terminus of the active state μOR, which forms a lid over the orthosteric binding site (residues Gly52–Met65) was removed before receptor preparation. Matching spheres were generated based on the pose of PZM21 in the inactive state. The resulting complexes were then minimized with AMBER. The pose of PZM21 in the active state μOR structure was further refined using Glide (Schrödinger) in XP mode.

Molecular dynamics simulations were based on crystal structures of μOR in the inactive- and active-state conformation (PDB: 4DKL and 5CM1, respectively). In both cases, all non-receptor residues (T4 lysozyme in the inactive state and Nb39 in the active state) were removed. For the active state, amino-terminal residues were removed as in the docking studies. Initial coordinates of PZM21 were generated by molecular docking as described above. The receptor was simulated with two tautomers of His297[6.52], either in the neutral Nδ or the Nε state. The μOR-PZM21 complex was embedded in a lipid bilayer consisting of dioleoylphosphatidylcholine (DOPC) molecules as described previously[47]. The charges of the inactive- and active-state simulation systems were neutralized by adding 11 and 14 chloride ions, respectively. To carry out MD simulations, the GROMACS package was used as described previously[70]. Briefly, the general AMBER force field (GAFF)[71] was used for PZM21 and the lipids and the AMBER force field ff99SB[72] for the receptor. Parameters for PZM21 were assigned using antechamber, and charges were calculated using Gaussian09 (Gaussian, Inc.) at the HF/6-31(d,p) level and the RESP procedure according to the literature[73]. During the simulations, PZM21 was protonated at its tertiary amine and simulated as a cation. The SPC/E water model[74] was used, and the simulations were carried out at 310 K. Analysis of the trajectories was performed using GROMACS. Each simulation in a given condition was initiated from identical coordinates, but with initial atom velocities assigned independently and randomly. An overview of the simulation systems and their simulation times is shown in the Supplementary Information.

Data analysis and reporting

Other than the *in vivo* studies, no statistical analysis was applied to *in vitro* or cell-based signalling assays. Sample size (number of assays for each compound or receptor) was predetermined to be in triplicate or quadruplicate for primary screening assays at a single concentration. For concentration-response assays, the sample size (number of assays for each compound at selected receptors) was also predetermined to be tested for a minimum of three assays, each in triplicate or quadruplicate. None of the functional assays were blinded to investigators.

Extended Data
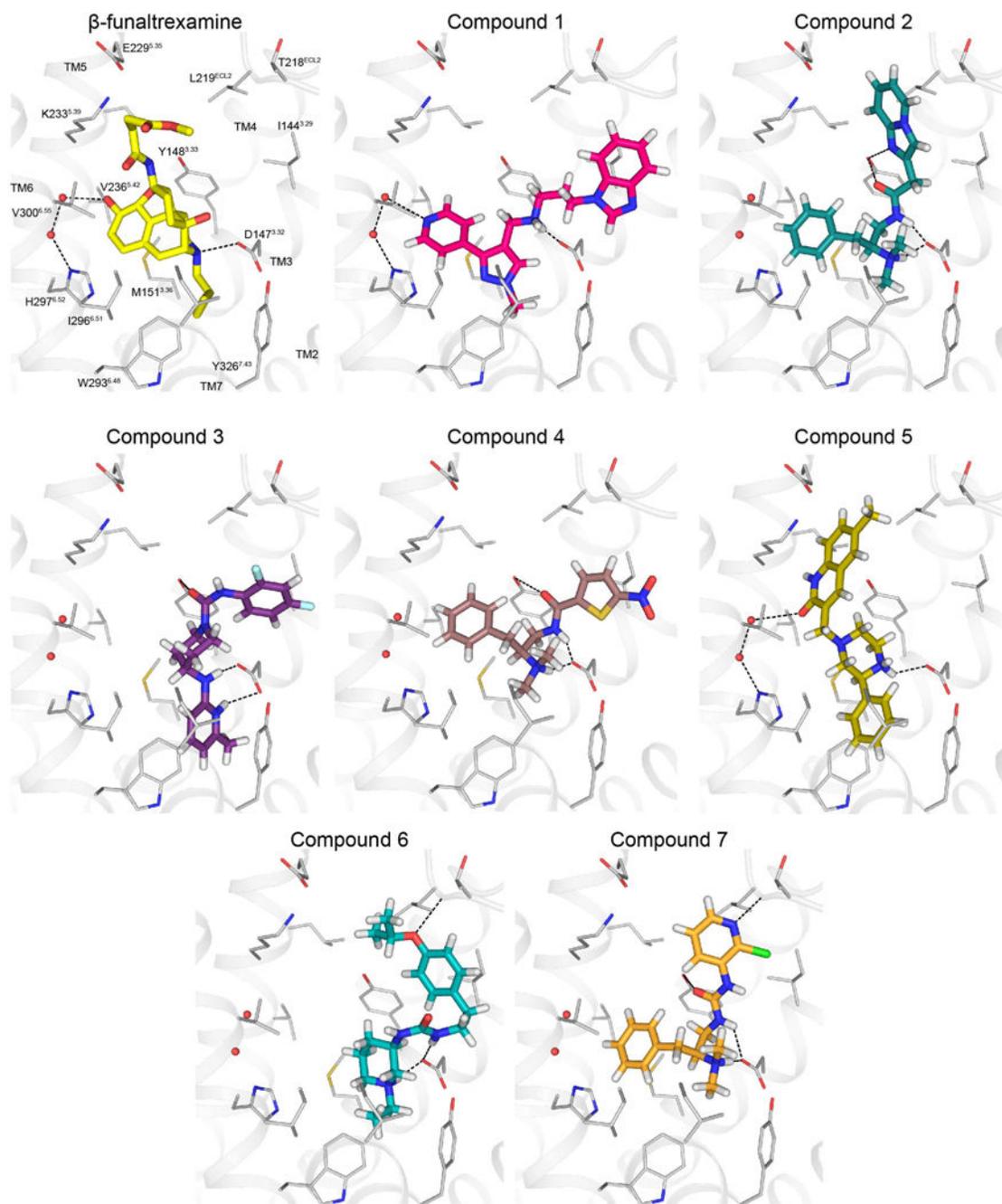
Extended Data Figure 1. Docking poses of active compounds

Seven of 23 experimentally tested compounds bound to the µOR with micromolar affinity. Their docked poses often occupy sites not exploited by the antagonist β-funaltrexamine. In each case, a canonical ionic interaction with D147$^{3.32}$ is observed.
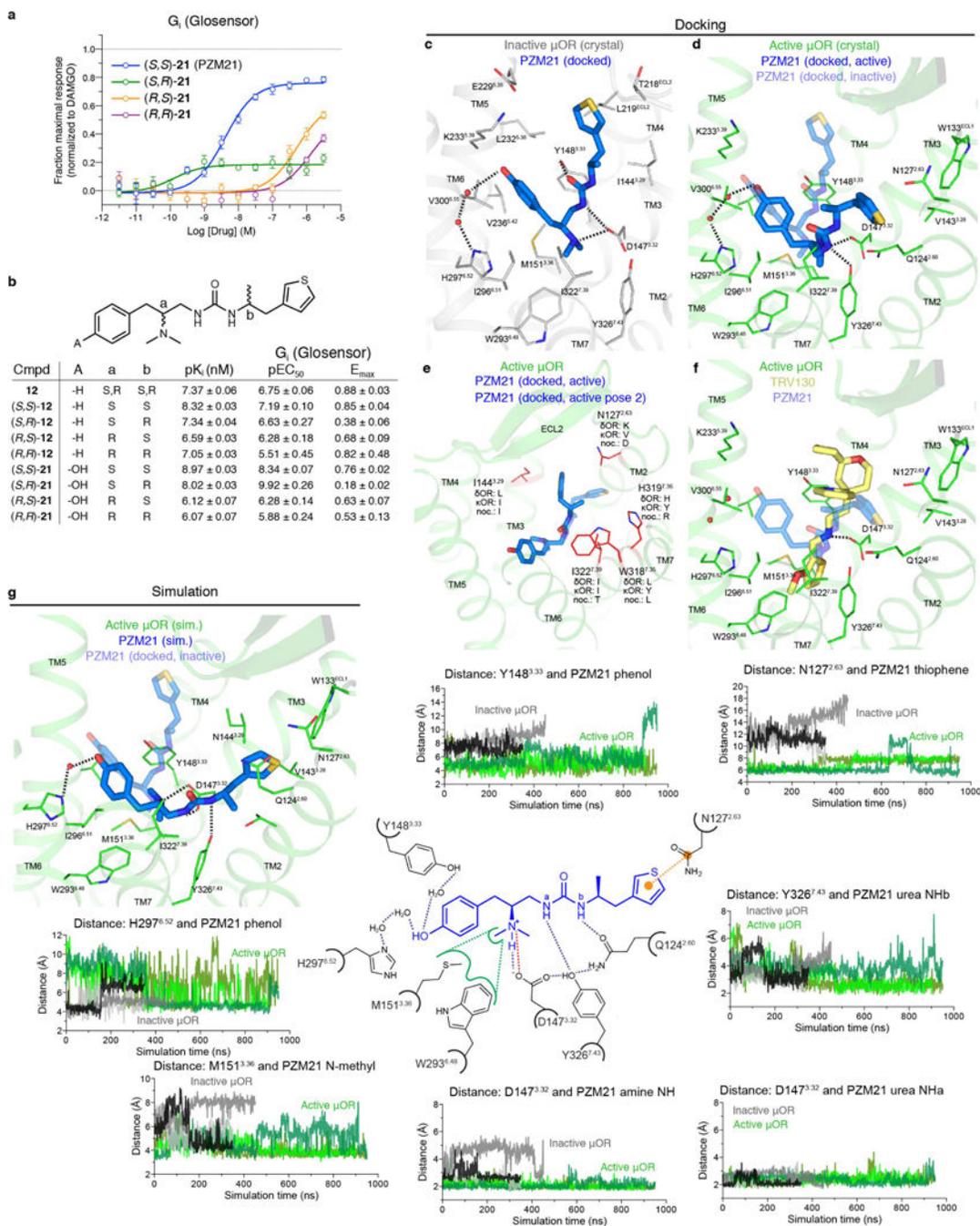
**Extended Data Figure 2. Stereochemical structure-activity relationship**

a, As with the different stereoisomers of **12**, variation of the chiral centres in compound PZM21 results in large changes in efficacy and potency. Data are mean ± s.e.m. of normalized results (*n = 3* measurements). **b**, Structure–activity relationship of compound **12** and **21** stereoisomers with affinities displayed as p*K*i values and agonist potency and efficacy in a $G_{i/o}$ Glosensor assay. **c, d**, PZM21 docked to active µOR shows a more extended conformation as compared to the inactive state. **e**, In the docked active state, the PZM21 thiophene extends into the specificity-determining region of opioid receptors. Key

interacting residues here are highlighted as red lines and corresponding residues at the other human opioid receptors are indicated. **f**, Docked pose of TRV130 within the μOR site, showing minimal overlap in key pharmacophores with PZM21 besides the ionic interaction between the cationic amine and D147[3.32]. **g**, Molecular dynamics simulations of PZM21 in the inactive μOR state (grey and black traces) leads to a stable conformation with the thiophene positioned > 10 Å away from N127[2.63] (total of 2 μs of simulation time over three independent trajectories). In contrast, PZM21 adopts a more extended pose when simulated with active μOR, with an average distance of 6 Å between the thiophene and N127[2.63]. Other key interactions between μOR and PZM21 are also highlighted.
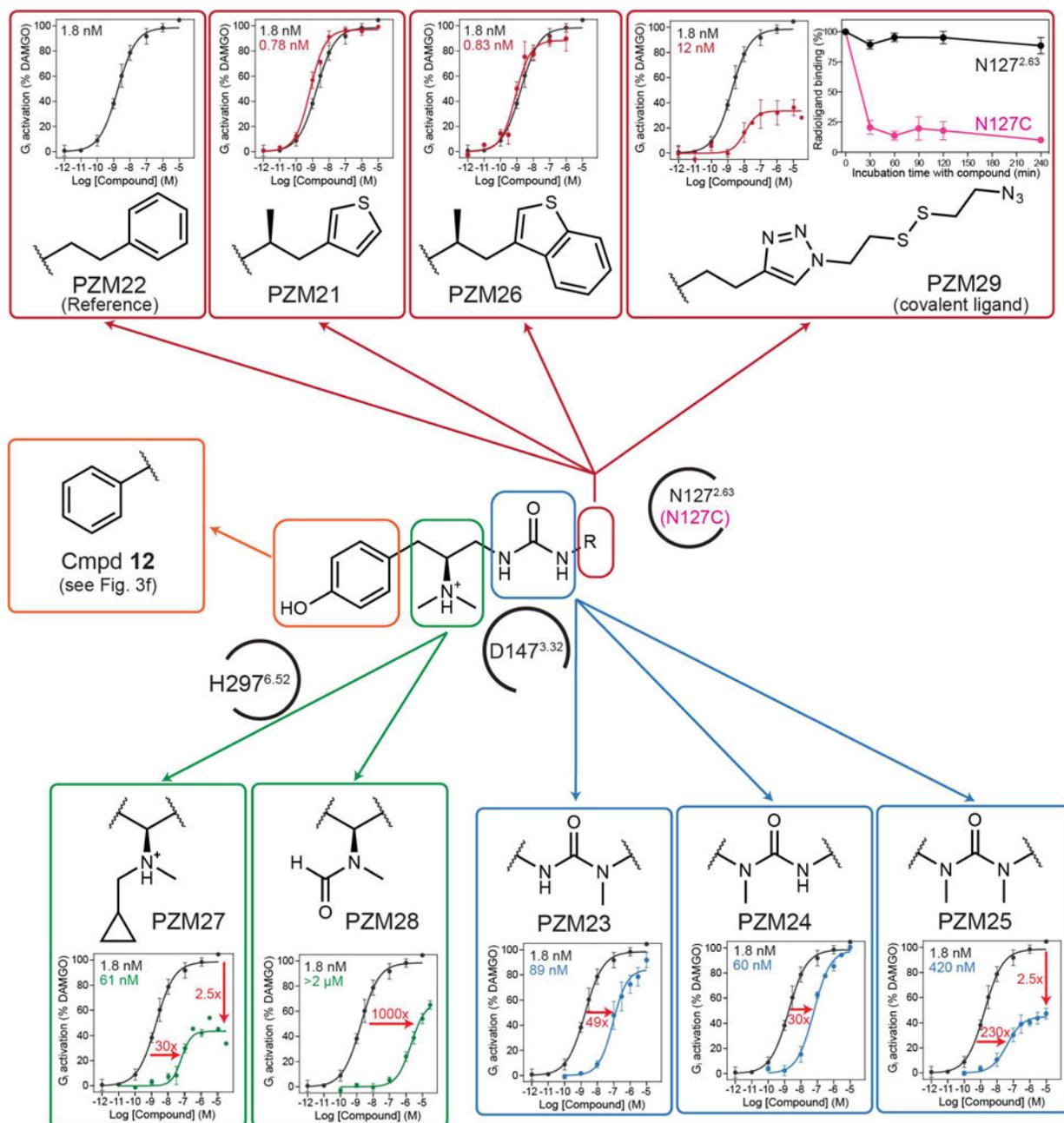
Extended Data Figure 3. Structure activity relationship defined by PZM21 analogues
Eight analogues were synthesized to probe the binding orientation of PZM21 and their efficacy as agonists was tested in a CAMYEL-based $G_{i/o}$ signalling assay. Analogues were compared to a parent reference compound (PZM22) with similar efficacy and potency to PZM21. In each case, the EC_{50} value for PZM22 is shown in black (1.8 nM) and the EC_{50} for the analogue is coloured. The covalent compound PZM29 binds to the μOR:N127C variant irreversibly, as evidenced by wash-resistant inhibition of radioligand binding. Signalling data are mean ± s.e.m. of normalized results (n = 3 measurements).
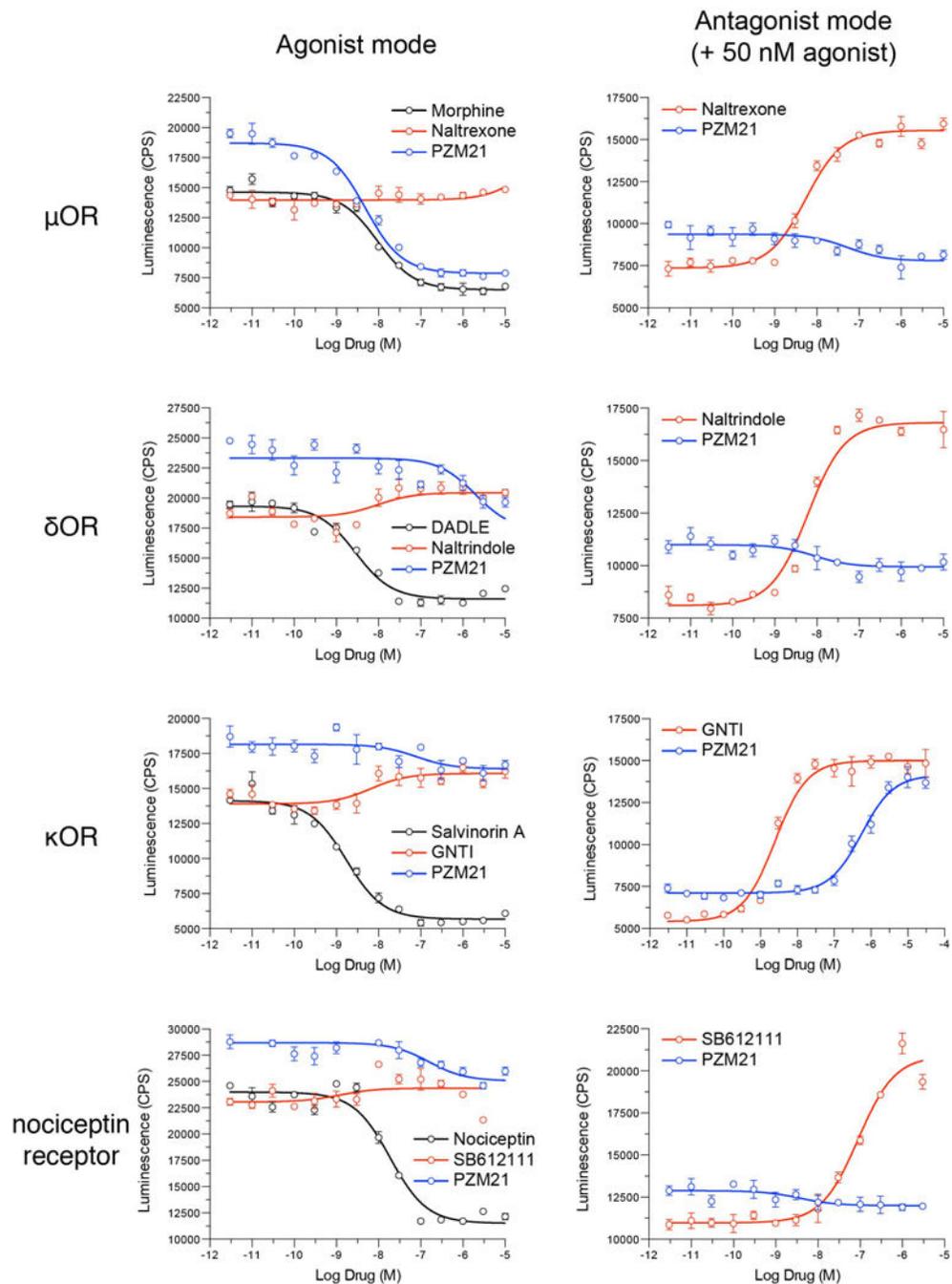
Extended Data Figure 4. Signalling properties of PZM21 at the opioid receptors
Displayed are raw luminescence data from a $G_{i/o}$ Glosensor assay. In agonist mode, agonists decrease luminescence while inverse agonists increase it by diminishing basal signalling. For each opioid receptor, a prototypical well-characterized agonist (black curves) and antagonist (red curves) were used to validate the assay. In antagonist mode, a competition reaction is performed with 50 nM agonist and an escalating amount of tested drug. Here, true antagonists increase the observed signal, consistent with their ability to compete with

the agonist but not induce G_i signalling. Data are mean ± s.e.m. of non-normalized results (n =3 measurements).
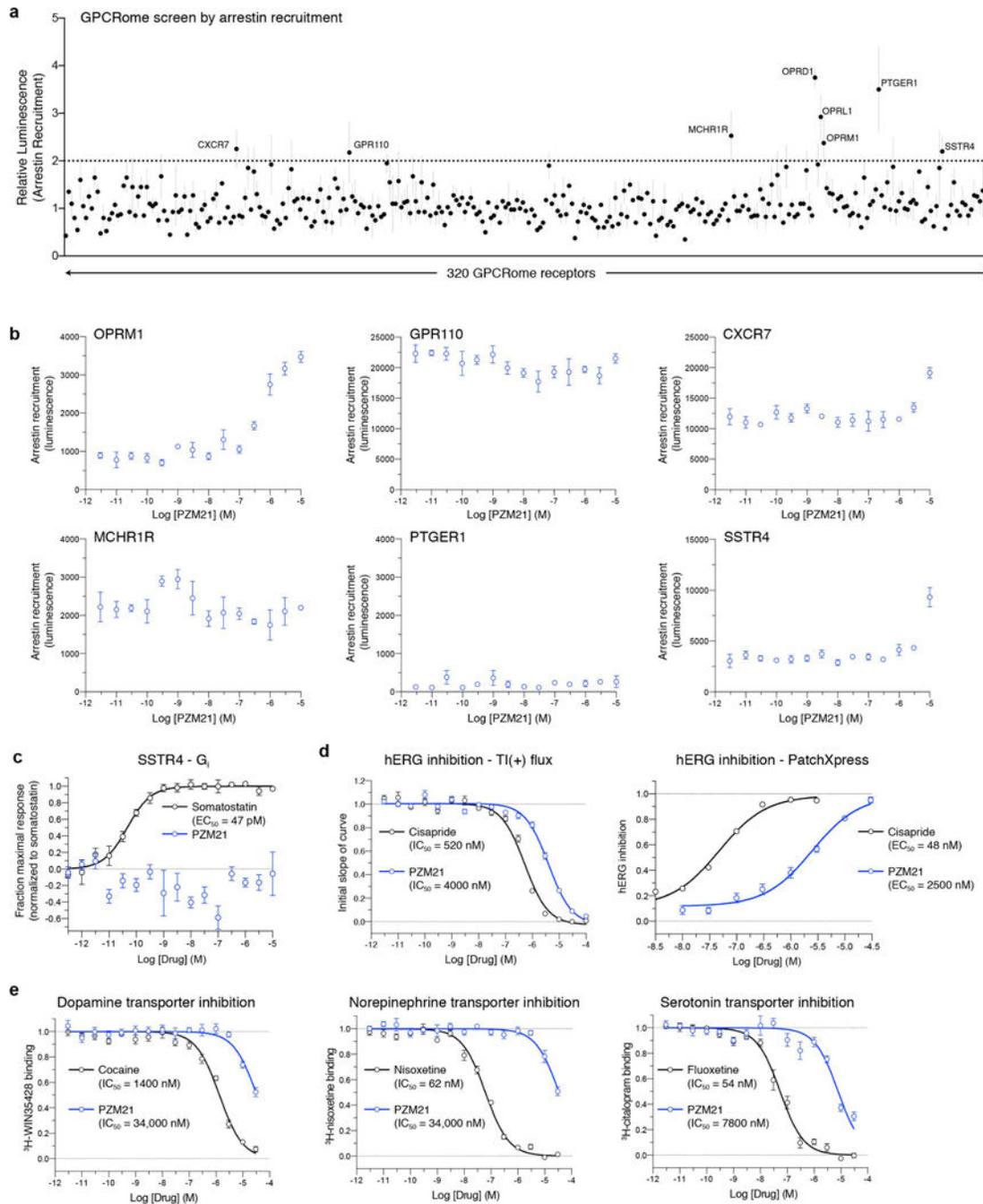
Extended Data Figure 5. PZM21 is selective for µOR

a, Compound PZM21 was screened against 320 non-olfactory GPCRs for agonism in the arrestin recruitment TANGO assay. Each point shows luminescence normalized to basal level at a given GPCR, with vertical lines indicating the standard error of the mean. **b,** GPCRs for which PZM21 induces an increase in signal twofold over background were

further tested in full dose–response mode. Several potential targets (GPR110, MCHR1R, PTGER1) did not show dose-dependent increase in signal and probably represent screening false positives. CXCR7 and SSTR4 did show dose-dependent signals at high concentrations of PZM21, and were further tested in non-arrestin signalling assays. **c**, PZM21 does not show a dose-dependent change in cAMP inhibition in a $G_{i/o}$ Glosensor assay measuring SSTR4 activation, indicating that the single elevated point in **b** is probably a false positive result. **d**, **e**, Inhibition assays of hERG (**d**) and the dopamine transporter (DAT), norepinephrine transporter (NET), and serotonin transporter (SERT) (**e**) show that PZM21 has weak inhibitory activity ranging from 2–34 μM at these targets. For **a**, data are mean ± s.e.m. of non-normalized results ($n = 4$ measurements). For **b**–**e**, data are mean ± s.e.m. of normalized results ($n = 3$–6 measurements).
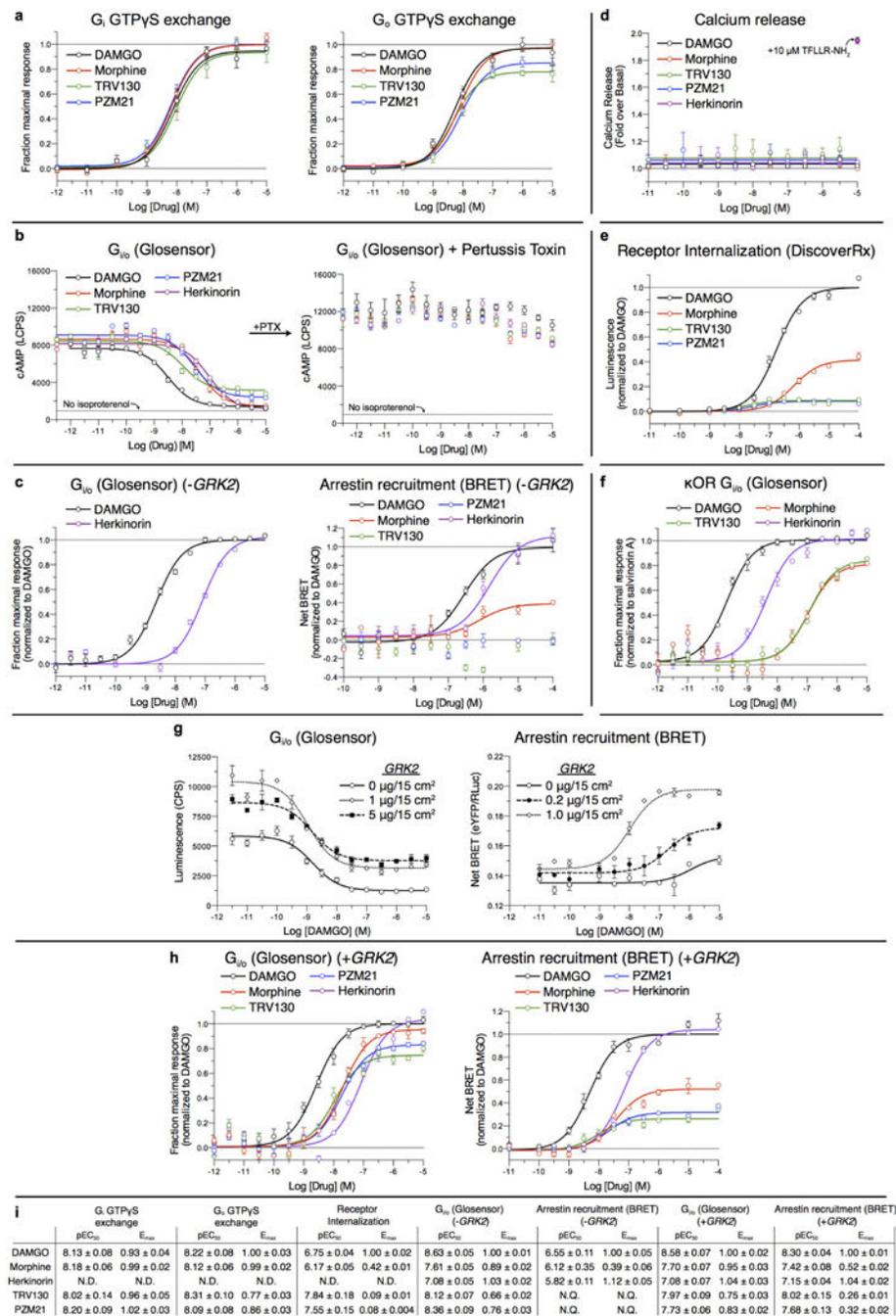
Extended Data Figure 6. Signalling profile of PZM21 and other μOR agonists
a, PZM21 is an efficacious G_i and G_o agonist in a GTP γS assay. **b**, Like other μOR agonists, PZM21 induces a dose-dependent decrease in cAMP levels that is sensitive to pertussis toxin, confirming $G_{i/o}$ mediated signalling. **c**, Herkinorin is a $G_{i/o}$ agonist and robustly recruits arrestin in a BRET assay performed in the absence of GRK2 overexpression. TRV130 or PZM21 show undetectable levels of arrestin recruitment in the same experiement. **d**, PZM21 and other opioids show no activity in a calcium-release assay, indicating no G_q-mediated second messenger signalling. The positive control TFLLR-NH2

efficiently activates the G_q coupled receptor PAR-1. **e**, PZM21 and TRV130 induce much decreased receptor internalization versus DAMGO and even morphine. **f**, Herkinorin and TRV130 are potent agonists of the κOR. PZM21 is a κOR antagonist (see Extended Data Fig. 4). **g**, In HEK293 cells, GRK2 expression levels have minimal effect on the potency and efficacy of the unbiased agonist DAMGO in a $G_{i/o}$ activation assay. Increased GRK2 levels change the basal cAMP signal due to increased desentization of μOR, which lowers receptor basal activity and leads to elevated isoproterenol-induced cAMP. In an arrestin-recruitment BRET assay, increased GRK2 expression increases both the potency and maximal efficacy of the unbiased agonist DAMGO. This is likely because GRK2 mediated phosphorylation is required for efficient β-arrestin recruitment. **h**, G_i activation and arrestin recruitment in cells co-expressing 1.0 μg/15 cm^2 of GRK2. Notably, PZM21 induces a higher maximal level of arrestin recruitment as compared to U2OS cells, which express very low levels of GRK2, but this level is significantly lower than morphine. Despite the lower efficacy for arrestin recruitment observed for morphine, TRV130 and PZM21 compared to DAMGO, a formal calculation of bias by the operational models fails to show that this effect is significant. **i**, Table of pEC_{50} values and E_{max} values for various signalling assays. All data are mean ± s.e.m. of results (n = 2–6 measurements).
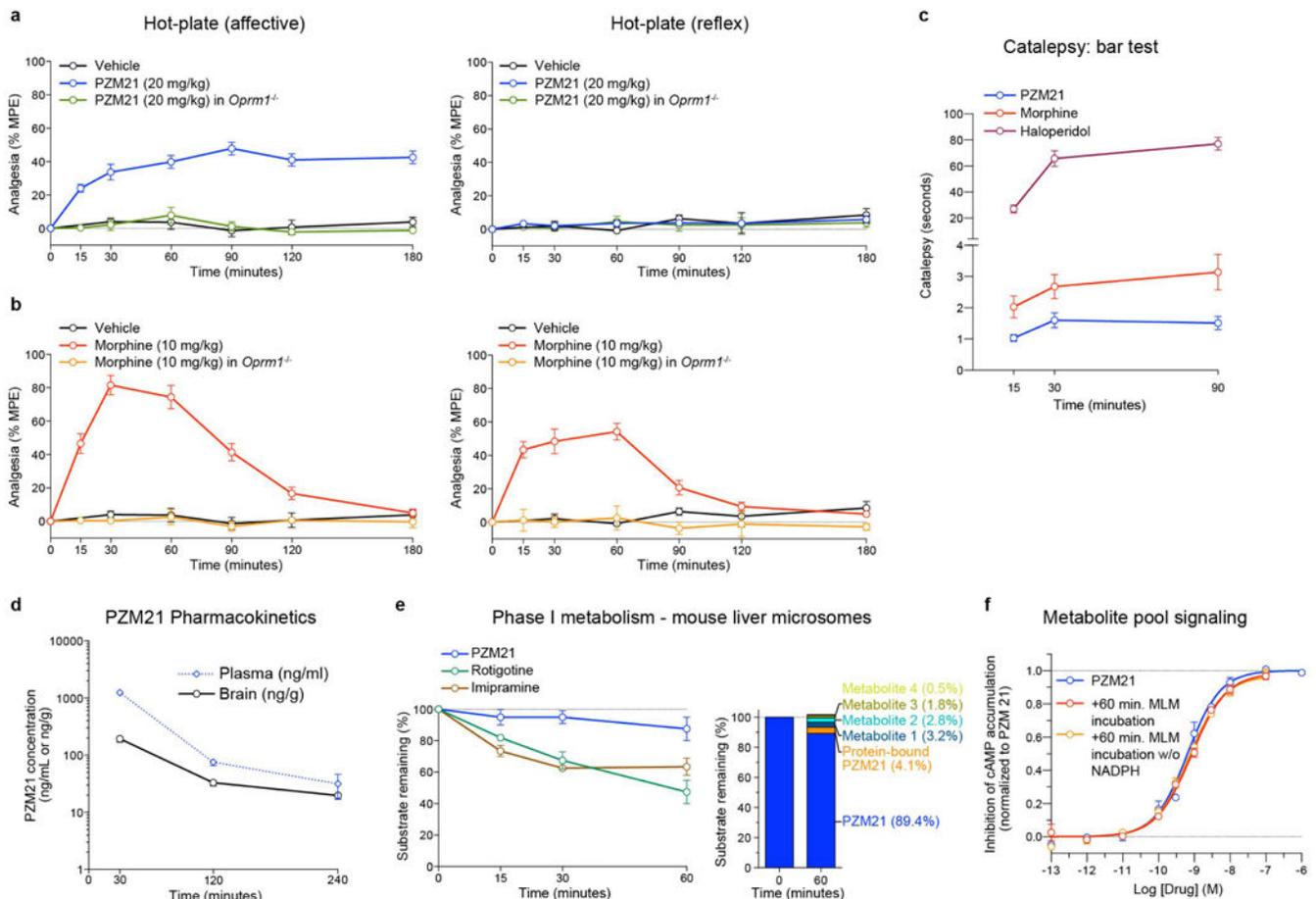
Extended Data Figure 7. Additional *in vivo* studies of PZM21

a, Analgesic responses measured in the hotplate assay were subcategorized into either affective or reflexive behaviours and scored separately. **b**, Morphine ($n = 10$ animals) induces changes in both behaviours, while PZM21 ($n = 13$ animals) only modulates the attending (affective) component. Knockout of the μOR ablates all analgesic responses by morphine and PZM21. **c**, PZM21 shows minimal cataleptic effect compared to morphine at different time points. The effect of haloperidol was included as a positive control. **d**, Pharmacokinetic studies of PZM21 ($n = 3$–4 animals for each time point) show central nervous system penetration of the compound, with a peak level of 197 ng of PZM21 per g of brain tissue. With a concomitant serum concentration of 1,253 ng/ml, this represents a serum:brain concentration ratio of 6.4. These levels are similar to those achieved by morphine, which shows a peak brain concentration of approximately 300 ng/g and a serum:brain concentration ratio of 3.7 30 min after subcutaneous injection[75]. **e**, Metabolism of PZM21 over 60 min exposure to mouse liver microsomes. Rotigotine and imipramine serve as positive controls for extensive phase I metabolism. The total amount of PZM21 and metabolite pool is slightly greater than 100% (101.8%) reflecting cumulative error in LC/MS analysis. **f**, A $G_{i/o}$ signalling assay shows that none of the metabolites are measurably more potent activators of the μOR versus PZM21 alone. The metabolite pool after the 60-min incubation was used directly in the signalling assay. As a negative control, the pooled material from a reaction carried out in the absence of the key cofactor NADPH was used in the signalling assay. All data are mean ±s.e.m. For **e**, reactions were run in triplicate and the s.e.m. was calculated from individual measurements of each reaction.

Extended Data Table 1

Molecules with μOR activity identified in the initial screen
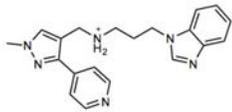
Cmpd	Structure	Rank	$T_c{}^a$	μOR K_i (μM)	Nearest ChEMBL μOR ligand
1		467	0.28	7.2	
2		358	0.28	5.8	
3		1281	0.30	13.8	
4		1465	0.30	2.3	
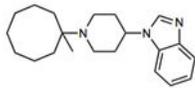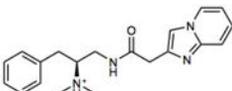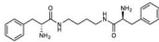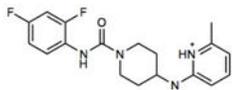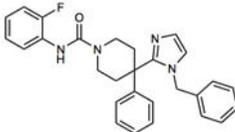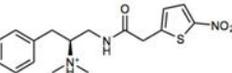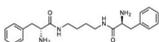
Cmpd	Structure	Rank	T_c^{a}	µOR K_i (µM)	Nearest ChEMBL µOR ligand
5		2418	0.31	4.7	
6		2211	0.30	10.0	
7		1140	0.30	2.5	

[a] The ECFP4 Tanimoto similarity (T_C) to the most similar µOR ligand in ChEMBL16.

Extended Data Table 2

Analogues tested at the µOR

Cmpd	Structure	Docking Score	T_c^{a}	µOR K_i (µM)	κOR K_i (µM)	µOR G_i EC50 (µM)	Nearest ChEMBL µOR ligand
8		−42.08	0.31	0.82	0.46	6.6	
9		−48.30	0.31	>10	1.36	N.A.[b]	
10		−51.73	0.31	4.75	>10	N.A.[b]	
11		−46.79	0.35	1.86	>10	N.A.[b]	
12		−51.88	0.35	0.042	0.46	0.18	

Cmpd	Structure	Docking Score	$T_c{}^a$	μOR K_i (μM)	κOR K_i (μM)	μOR G_i EC50 (μM)	Nearest ChEMBL μOR ligand
13		−51.22	0.35	0.550	1.02	3.1	
14		−50.42	0.37	0.087	0.51	0.44	
15		−43.17	0.37	0.130	>10	N.A.[b]	
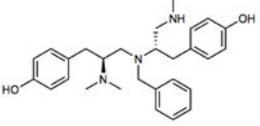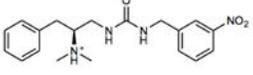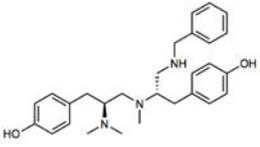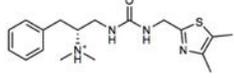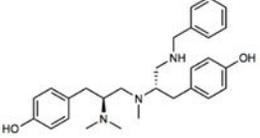
[a] The ECFP4 Tanimoto similarity (T_C) to the most similar μOR ligand in ChEMBL16.

[b] No measurable activity.

Extended Data Table 3

Binding and signalling properties of compounds 12 and PZM21

	12	PZM21
K_i(nM)		
μOR	42	1.1
δOR	N.A.	506
κOR	464	18
nociceptin	N.D.[a]	N.D.[a]
$G_{i/o}$ (Glosensor)		
EC$_{50}$(nM)|E$_{max}$(%)		
μOR	180 | 88	4.6 | 77
δOR	N.A.[b]	1900 | 78
κOR	N.A.[b]	N.A.[b]
nociceptin	1400 | 43	N.A.[b]
Arrestin recruitment (PathHunter)		
EC$_{50}$(nM)|E$_{max}$(%)		
μOR	940 | 9.4	NA.[a]

[a] Not determined.

[b] No measurable activity.

Supplementary Material

Refer to Web version on PubMed Central for supplementary material.

Acknowledgments

References

1. Lord JAH, Waterfield AA, Hughes J, Kosterlitz HW. Endogenous opioid peptides: multiple agonists and receptors. Nature. 1977; 267:495–499. [PubMed: 195217]

2. Martin WR, Eades CG, Thompson JA, Huppler RE, Gilbert PE. The effects of morphine- and nalorphine-like drugs in the nondependent and morphine-dependent chronic spinal dog. J Pharmacol Exp Ther. 1976; 197:517–532. [PubMed: 945347]

3. Hughes J, et al. Identification of two related pentapeptides from the brain with potent opiate agonist activity. Nature. 1975; 258:577–580. [PubMed: 1207728]

4. Bohn LM, Gainetdinov RR, Lin FT, Lefkowitz RJ, Caron MG. μ-opioid receptor desensitization by β-arrestin-2 determines morphine tolerance but not dependence. Nature. 2000; 408:720–723. [PubMed: 11130073]

5. Bohn LM, et al. Enhanced morphine analgesia in mice lacking β-arrestin 2. Science. 1999; 286:2495–2498. [PubMed: 10617462]

6. Raehal KM, Walker JK, Bohn LM. Morphine side effects in β-arrestin 2 knockout mice. J Pharmacol Exp Ther. 2005; 314:1195–1201. [PubMed: 15917400]

7. DeWire SM, et al. A G protein-biased ligand at the μ-opioid receptor is potently analgesic with reduced gastrointestinal and respiratory dysfunction compared with morphine. J Pharmacol Exp Ther. 2013; 344:708–717. [PubMed: 23300227]

8. Soergel DG, et al. Biased agonism of the μ-opioid receptor by TRV130 increases analgesia and reduces on-target adverse effects versus morphine: a randomized, double-blind, placebo-controlled, crossover study in healthy volunteers. Pain. 2014; 155:1829–1835. [PubMed: 24954166]

9. Manglik A, et al. Crystal structure of the μ-opioid receptor bound to a morphinan antagonist. Nature. 2012; 485:321326.

10. Granier S, et al. Structure of the δ-opioid receptor bound to naltrindole. Nature. 2012; 485:400–404. [PubMed: 22596164]

11. Wu H, et al. Structure of the human κ-opioid receptor in complex with JDTic. Nature. 2012; 485:327–332. [PubMed: 22437504]

12. Thompson AA, et al. Structure of the nociceptin/orphanin FQ receptor in complex with a peptide mimetic. Nature. 2012; 485:395–399. [PubMed: 22596163]

13. Carlsson J, et al. Ligand discovery from a dopamine D3 receptor homology model and crystal structure. Nat Chem Biol. 2011; 7:769–778. [PubMed: 21926995]

14. de Graaf C, et al. Crystal structure-based virtual screening for fragment-like ligands of the human histamine H_1 receptor. J Med Chem. 2011; 54:8195–8206. [PubMed: 22007643]

15. Katritch V, et al. Structure-based discovery of novel chemotypes for adenosine A_{2A} receptor antagonists. J Med Chem. 2010; 53:1799–1809. [PubMed: 20095623]

16. Kolb P, et al. Structure-based discovery of β2-adrenergic receptor ligands. Proc Natl Acad Sci USA. 2009; 106:6843–6848. [PubMed: 19342484]

17. Langmead CJ, et al. Identification of novel adenosine A_{2A} receptor antagonists by virtual screening. J Med Chem. 2012; 55:1904–1909. [PubMed: 22250781]

18. Powers RA, Morandi F, Shoichet BK. Structure-based discovery of a novel, noncovalent inhibitor of AmpC β-lactamase. Structure. 2002; 10:1013–1023. [PubMed: 12121656]

19. Huang XP, et al. Allosteric ligands for the pharmacologically dark receptors GPR68 and GPR65. Nature. 2015; 527:477–483. [PubMed: 26550826]

20. Irwin JJ, Sterling T, Mysinger MM, Bolstad ES, Coleman RG. ZINC: a free tool to discover chemistry for biology. J Chem Inf Model. 2012; 52:1757–1768. [PubMed: 22587354]

21. Mysinger MM, Shoichet BK. Rapid context-dependent ligand desolvation in molecular docking. J Chem Inf Model. 2010; 50:1561–1573. [PubMed: 20735049]

22. Mysinger MM, et al. Structure-based ligand discovery for the protein–protein interface of chemokine receptor CXCR4. Proc Natl Acad Sci USA. 2012; 109:5517–5522. [PubMed: 22431600]

23. Negri A, et al. Discovery of a novel selective kappa-opioid receptor agonist using crystal structure-based virtual screening. J Chem Inf Model. 2013; 53:521–526. [PubMed: 23461591]

24. Ballesteros JA, Weinstein H. Integrated methods for the construction of three-dimensional models and computational probing of structure-function relations in G protein-coupled receptors. Methods in Neurosciences. 1995; 25:366–428.

25. Gaulton A, et al. ChEMBL: a large-scale bioactivity database for drug discovery. Nucleic Acids Res. 2012; 40:D1100–D1107. [PubMed: 21948594]

26. Muchmore SW, et al. Application of belief theory to similarity data fusion for use in analog searching and lead hopping. J Chem Inf Model. 2008; 48:941–948. [PubMed: 18416545]

27. Pasternak GW, Pan YX. μ opioids and their receptors: evolution of a concept. Pharmacol Rev. 2013; 65:1257–1317. [PubMed: 24076545]

28. Fenalti G, et al. Structural basis for bifunctional peptide recognition at human δ-opioid receptor. Nat Struct Mol Biol. 2015; 22:265–268. [PubMed: 25686086]

29. Huang W, et al. Structural insights into μ-opioid receptor activation. Nature. 2015; 524:315–321. [PubMed: 26245379]

30. Kroeze WK, et al. PRESTO-Tango as an open-source resource for interrogation of the druggable human GPCRome. Nat Struct Mol Biol. 2015; 22:362–369. [PubMed: 25895059]

31. Kenakin T, Christopoulos A. Signalling bias in new drug discovery: detection, quantification and therapeutic impact. Nat Rev Drug Discov. 2013; 12:205–216. [PubMed: 23411724]

32. Nickolls SA, Humphreys S, Clark M, McMurray G. Co-expression of GRK2 reveals a novel conformational state of the μ-opioid receptor. PLoS One. 2013; 8:e83691. [PubMed: 24376730]

33. Groer CE, et al. An opioid agonist that does not induce μ-opioid receptor–arrestin interactions or receptor internalization. Mol Pharmacol. 2007; 71:549–557. [PubMed: 17090705]

34. Le Bars D, Gozariu M, Cadden SW. Animal models of nociception. Pharmacol Rev. 2001; 53:597–652. [PubMed: 11734620]

35. Li C, et al. μ opioid receptor modulation of dopamine neurons in the periaqueductal gray/dorsal raphe: a role in regulation of pain. Neuropsychopharmacology. 2016; 41:2122–2132. [PubMed: 26792442]

36. Han S, Soleiman MT, Soden ME, Zweifel LS, Palmiter RD. Elucidating an affective pain circuit that creates a threat memory. Cell. 2015; 162:363–374. [PubMed: 26186190]

37. Gogas KR, Presley RW, Levine JD, Basbaum AI. The antinociceptive action of supraspinal opioids results from an increase in descending inhibitory control: correlation of nociceptive behavior and c-fos expression. Neuroscience. 1991; 42:617–628. [PubMed: 1659673]

38. Montandon G, et al. G-protein-gated inwardly rectifying potassium channels modulate respiratory depression by opioids. Anesthesiology. 2016; 124:641–650. [PubMed: 26675532]

39. Spanagel R, Herz A, Shippenberg TS. Opposing tonically active endogenous opioid systems modulate the mesolimbic dopaminergic pathway. Proc Natl Acad Sci USA. 1992; 89:2046–2050. [PubMed: 1347943]

40. Bohn LM, et al. Enhanced rewarding properties of morphine, but not cocaine, in β(arrestin)-2 knock-out mice. J Neurosci. 2003; 23:10265–10273. [PubMed: 14614085]

41. Tzschentke TM. Measuring reward with the conditioned place preference paradigm: a comprehensive review of drug effects, recent progress and new issues. Prog Neurobiol. 1998; 56:613–672. [PubMed: 9871940]

42. Weiss DR, et al. Conformation guides molecular efficacy in docking screens of activated β-2 adrenergic G protein coupled receptor. ACS Chem Biol. 2013; 8:1018–1026. [PubMed: 23485065]

43. Carlsson J, et al. Structure-based discovery of A2A adenosine receptor ligands. J Med Chem. 2010; 53:3748–3755. [PubMed: 20405927]

44. Irwin JJ, et al. Automated docking screens: a feasibility study. J Med Chem. 2009; 52:5712–5720. [PubMed: 19719084]

45. Besnard J, et al. Automated design of ligands to polypharmacological profiles. Nature. 2012; 492:215–220. [PubMed: 23235874]

46. Weichert D, et al. Covalent agonists for studying G protein-coupled receptor activation. Proc Natl Acad Sci USA. 2014; 111:10744–10748. [PubMed: 25006259]

47. Möller D, et al. Functionally selective dopamine D$_2$, D$_3$ receptor partia agonists. J Med Chem. 2014; 57:4861–4875. [PubMed: 24831693]

48. Hübner H, Haubmann C, Utz W, Gmeiner P. Conjugated enynes as nonaromatic catechol bioisosteres: synthesis, binding experiments, and computational studies of novel dopamine receptor agonists recognizing preferentially the D$_3$ subtype. J Med Chem. 2000; 43:756–762. [PubMed: 10691700]

49. Lane JR, Powney B, Wise A, Rees S, Milligan G. G protein coupling and ligand selectivity of the D2L and D3 dopamine receptors. J Pharmacol Exp Ther. 2008; 325:319–330. [PubMed: 18218829]

50. Jiang LI, et al. Use of a cAMP BRET sensor to characterize a novel regulation of cAMP by the sphingosine 1-phosphate/G13 pathway. J Biol Chem. 2007; 282:10576–10584. [PubMed: 17283075]

51. Nakajima, K-i; Gimenez, LD.; Gurevich, V.; Wess, J. Designer Receptors Exclusively Activated by Designer Drugs. In: Thiel, G., editor. Neuromethods. Vol. 108. Springer; New York: 2015. p. 29-48.Ch. 2

52. Rajagopal S, et al. Quantifying ligand bias at seven-transmembrane receptors. Mol Pharmacol. 2011; 80:367–377. [PubMed: 21610196]

53. Rajagopal S. Quantifying biased agonism: understanding the links between affinity and efficacy. Nat Rev Drug Discov. 2013; 12:483.

54. Huang XP, Mangano T, Hufeisen S, Setola V, Roth BL. Identification of human Ether-à-go-go related gene modulators by three screening platforms in an academic drug-discovery setting. Assay Drug Dev Technol. 2010; 8:727–742. [PubMed: 21158687]

55. Balter RE, Dykstra LA. Thermal sensitivity as a measure of spontaneous morphine withdrawal in mice. J Pharmacol Toxicol Methods. 2013; 67:162–168. [PubMed: 23416790]

56. Sorge RE, et al. Olfactory exposure to males, including men, causes stress and related analgesia in rodents. Nat Methods. 2014; 11:629–632. [PubMed: 24776635]

57. Woolf CJ. Long term alterations in the excitability of the flexion reflex produced by peripheral tissue injury in the chronic decerebrate rat. Pain. 1984; 18:325–343. [PubMed: 6728499]

58. Blanchard RJ, Blanchard DC. Passive and active reactions to fear-eliciting stimuli. J Comp Physiol Psychol. 1969; 68:129–135. [PubMed: 5793861]

59. Bolles RC. Species-specific defense reactions and avoidance learning. Psychol Rev. 1970; 77:32.

60. Bolles RC, Fanselow MS. A perceptual-defensive-recuperative model of fear and pain. Behav Brain Sci. 1980; 3:291–301.

61. Estes WK. Discriminative conditioning; effects of a Pavlovian conditioned stimulus upon a subsequently established operant response. J Exp Psychol. 1948; 38:173–177. [PubMed: 18913666]

62. Estes WK, Skinner BF. Some quantitative properties of anxiety. J Exp Psychol. 1941; 29:390.

63. Rescorla RA, Lolordo VM. Inhibition of avoidance behavior. J Comp Physiol Psychol. 1965; 59:406–412. [PubMed: 14313781]

64. Skinner, BF. The behavior of organisms; an experimental analysis. D. Appleton-Century Company Incorporated; 1938.

65. Hunskaar S, Hole K. The formalin test in mice: dissociation between inflammatory and non-inflammatory pain. Pain. 1987; 30:103–114. [PubMed: 3614974]

66. Clougherty JE, et al. Chronic social stress and susceptibility to concentrated ambient fine particles in rats. Environ Health Perspect. 2010; 118:769–775. [PubMed: 20194079]

67. Sanberg PR, Bunsey MD, Giordano M, Norman AB. The catalepsy test: its ups and downs. Behav Neurosci. 1988; 102:748–759. [PubMed: 2904271]

68. Hiller C, et al. Functionally selective dopamine D2/D3 receptor agonists comprising an enyne moiety. J Med Chem. 2013; 56:5130–5141. [PubMed: 23730937]

69. Case, D., et al. AMBER 15. San Francisco, CA: University of California; 2015.

70. Goetz A, Lanig H, Gmeiner P, Clark T. Molecular dynamics simulations of the effect of the G-protein and diffusible ligands on the β2-adrenergic receptor. J Mol Biol. 2011; 414:611–623. [PubMed: 22037586]

71. Wang J, Wolf RM, Caldwell JW, Kollman PA, Case DA. Development and testing of a general amber force field. J Comput Chem. 2004; 25:1157–1174. [PubMed: 15116359]

72. Hornak V, et al. Comparison of multiple amber force fields and development of improved protein backbone parameters. Proteins. 2006; 65:712–725. [PubMed: 16981200]

73. Bayly CI, Cieplak P, Cornell W, Kollman PA. A well-behaved electrostatic potential based method using charge restraints for deriving atomic charges: the RESP model. J Phys Chem. 1993; 97:10269–10280.

74. Berendsen H, Grigera J, Straatsma T. The missing term in effective pair potentials. J Phys Chem. 1987; 91:6269–6271.

75. Kissin I, Brown PT, Robinson CA, Bradley EL. Acute tolerance in morphine analgesia continuous infusion and single injection in rats. Anesthesiology. 1991; 74:166–171. [PubMed: 1986642]
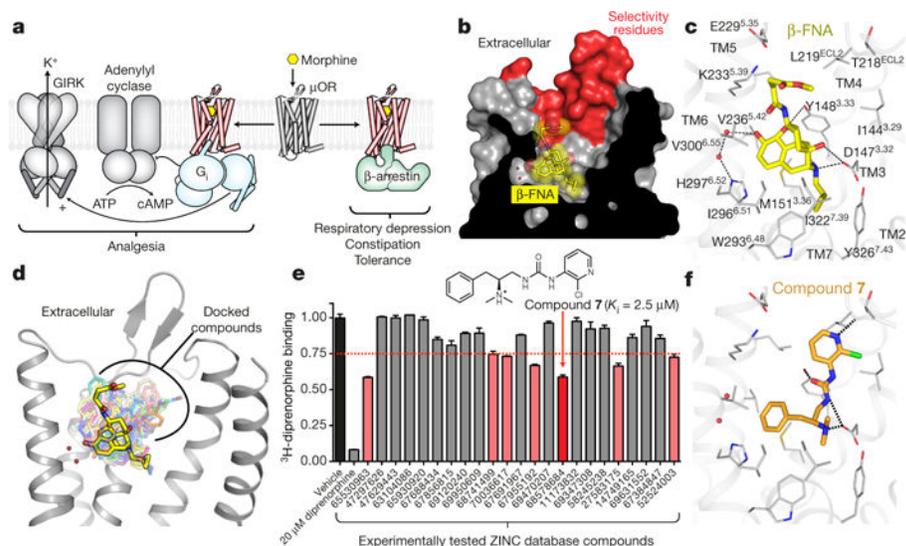
Figure 1. Structure based ligand discovery for the μOR

a, Opiate-induced μOR signalling through G_i activates G-protein-gated inwardly rectifying potassium channels (GIRKs) and inhibits adenylyl cyclase, leading to analgesia. Conversely, recruitment of β-arrestin is implicated in tolerance, respiratory depression, and constipation. **b**, Cutaway of the μOR orthosteric site to which β-FNA binds. Highlighted regions on the extracellular side diverge between the opioid receptors. **c**, Conserved features of opioid ligand recognition in the μOR. **d**, Overlaid docking poses of 23 compounds selected for experimental testing. **e**, Single-point competition binding assay of 23 candidate molecules against the μOR antagonist ^{3}H-diprenorphine. Each ligand was tested at 20 μM and for those with > 25% inhibition affinity was calculated in full displacement curves; data represent mean ± s.e.m. ($n = 3$ measurements). One of these hits, compound **7**, was subsequently optimized. **f**, Docking pose of compound **7**.
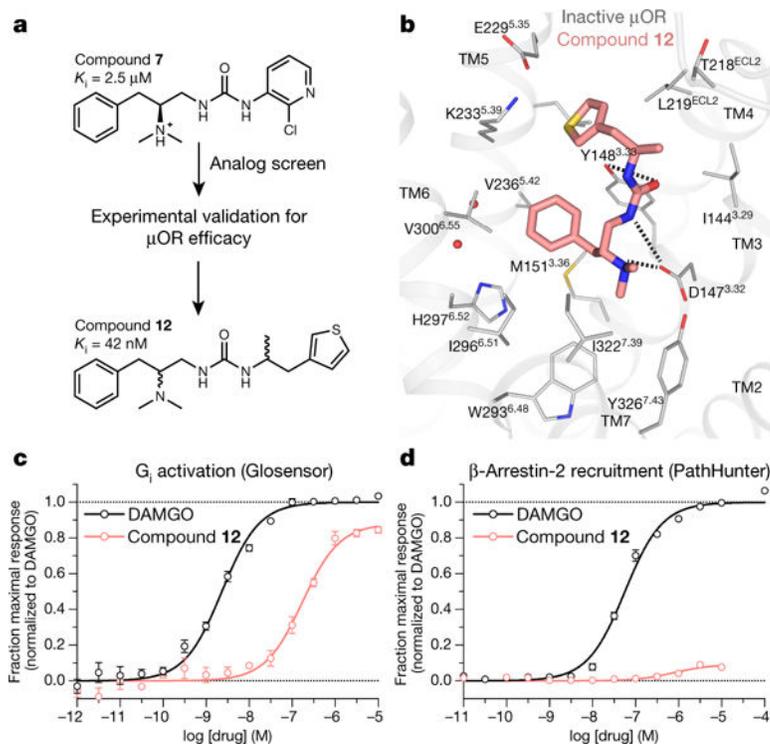
Figure 2. Discovery of a novel $G_{i/o}$-biased µOR agonist

a, Compound **12** was identified among a series of analogues to compound **7** and further investigated due to its µOR specificity and efficacy as a µOR agonist. **b**, Docking pose of Compound **12**. **c**, Compound **12** is a µOR agonist in a $G_{i/o}$ signalling assay with an EC_{50} of 180 nM. DAMGO is a prototypical unbiased opioid agonist. **d**, Despite robust activation of $G_{i/o}$, compound **12** induces minimal arrestin recruitment as compared to DAMGO. For **c**, **d**, data are mean ± s.e.m. of normalized results ($n = 3$–6 measurements).
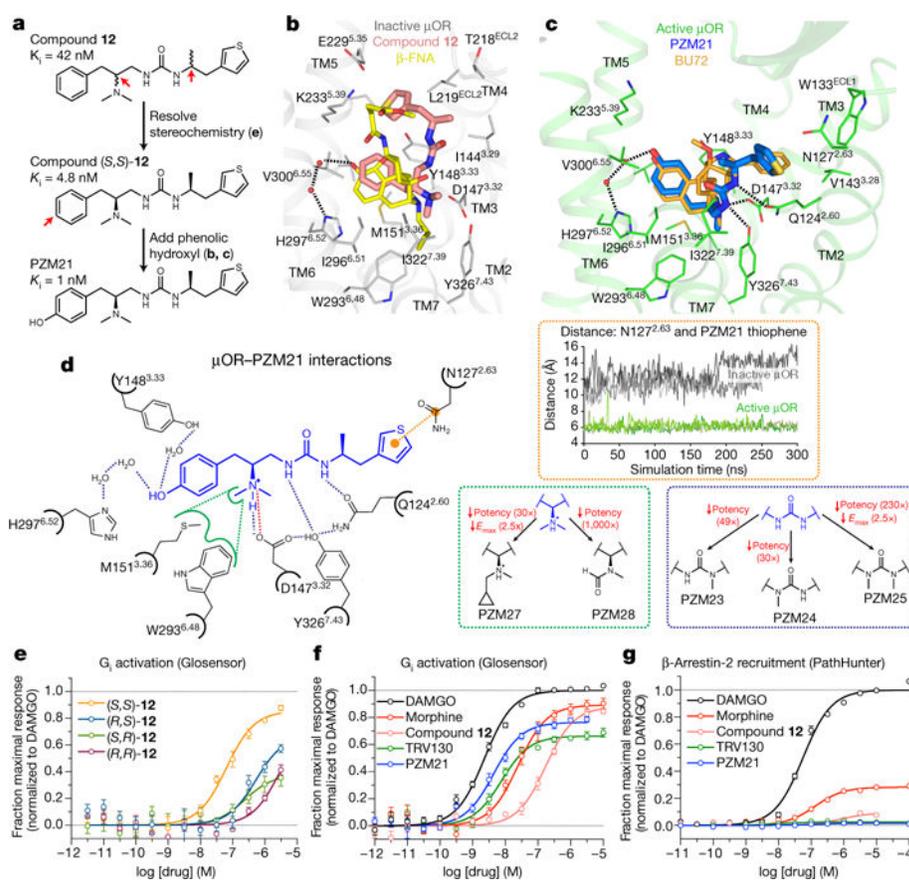
Figure 3. Structure-guided optimization towards a potent biased μOR agonist

a, Structure guided optimization towards PZM21. **b**, Docking pose of **12** compared to β-FNA. The phenolic hydroxyl of β-FNA coordinates His297[6.52] with two water molecules, providing an optimization strategy for **12**. **c**, PZM21 docked to active μOR with a water-mediated network between the PZM21 phenol and His297[6.52]. The co-crystallized agonist BU72 is shown as orange sticks. **d**, μOR–PZM21 interactions include hydrogen bonds (blue dash), hydrophobic interactions (green dash), and an ionic bond (red dash). Insets show select data from structure–activity relationship and molecular dynamics studies presented in more detail in Extended Data. **e**, Stereoisomers of **12** in a $G_{i/o}$ signalling assay. **f**, $G_{i/o}$ signalling assay shows robust μOR agonist activity for PZM21. **g**, PZM21 shows undetectable β-arrestin-2 recruitment in the PathHunter assay. For **e–g**, data are mean ± s.e.m. of normalized results ($n = 3$–6 measurements).
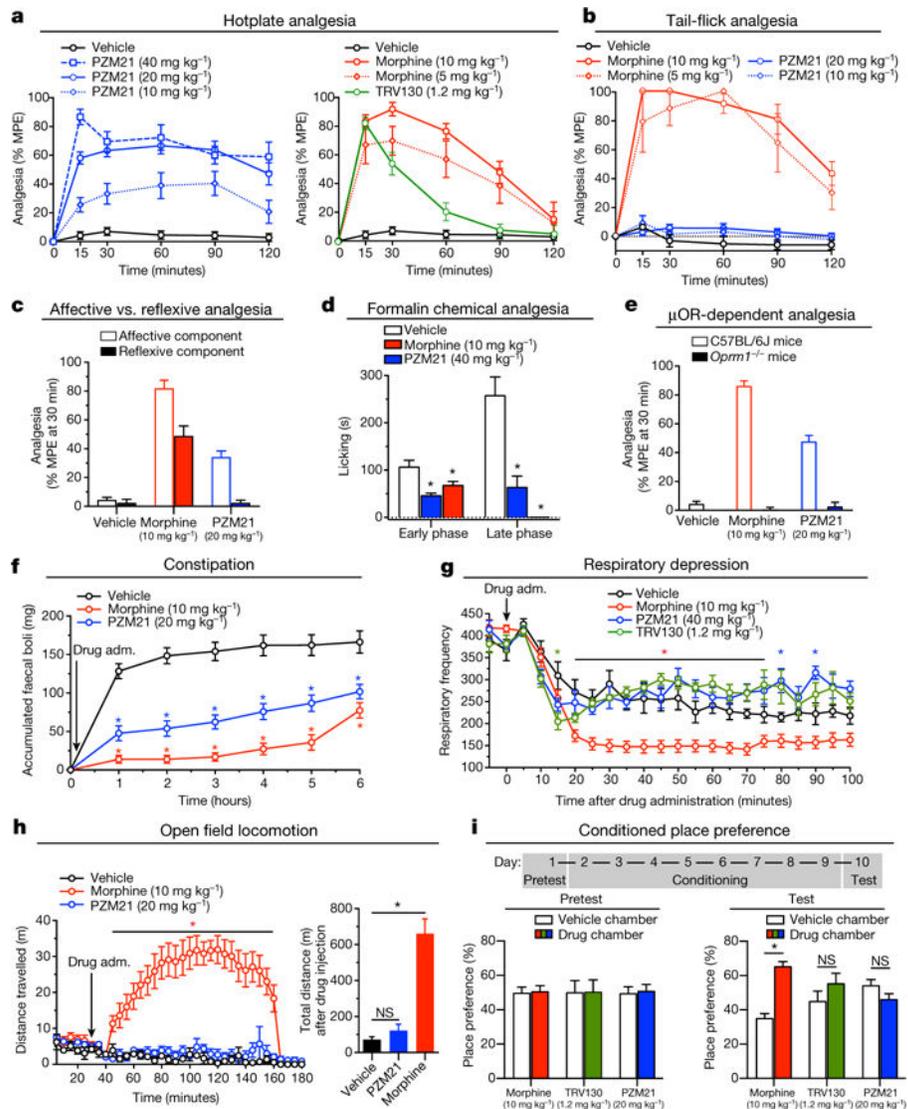
Figure 4. PZM21 is an analgesic with reduced on-target liabilities

a, Analgesia in the mouse hotplate assay. Latency of withdrawal to noxious stimuli is shown as percentage of the maximal possible effect (% MPE). The highest dose of PZM21 (40 mg kg^{-1}) yields an equi-analgesic response to 10 mg kg^{-1} morphine and 1.2 mg kg^{-1} TRV130 at 15 min. **b**, Compared to morphine, PZM21 shows no analgesia in the tail-flick assay. **c**, Unlike morphine, PZM21 decreases affective pain perception with minimal effect on reflexive pain. **d**, PZM21 and morphine produce sustained analgesia in a formalin injection nociception assay **e**, PZM21 shows no analgesic effect in *Oprm1$^{-/-}$* mice, supporting engagement of μOR *in vivo.* **f**, Constipatory effects of morphine and PZM21 compared to vehicle assessed by accumulated faecal boli. **g**, Whole-body mouse plethysmography shows decrease in respiratory frequency for morphine starting 20 min after administration of drug. An equi-analgesic dose of PZM21 has no effect on respiration versus vehicle, while TRV130 induces transient respiratory depression at 15 min. **h**, Open field locomotor assay. **i**, Place preference is induced by conditioning with 10 mg kg^{-1} morphine but not with 20 mg kg^{-1}

PZM21 nor with 1.2 mg kg^{-1} TRV130. Per cent of time spent in either vehicle or drug chamber before (pretest) or after (test) conditioning regimen. All data are mean ± s.e.m. and asterisks indicate statistically significant differences between drug and vehicle. The number of animals in each group and statistical tests are described in the Methods.